

1

2 A revised pan-Arctic permafrost soil Hg pool, based on western Siberia peat Hg 3 and carbon observations

4

5 Artem G. LIM¹, MARTIN JISKRA², Jeroen E. SONKE³,

6 Sergey V. LOIKO¹, NATALIA KOSYKH⁴, Oleg S. POKROVSKY^{3,5*}

7

⁸ *¹ BIO-GEO-CLIM Laboratory, Tomsk State University, Tomsk, Russia*

⁹ ² University of Basel, Environmental Geosciences, Bernoullistrasse 30, 4056 Basel, Switzerland

³ *Geosciences and Environment Toulouse, UMR 5563 CNRS, 14 Avenue Edouard Belin 31400*

11 *Toulouse, France*

⁴ *Lab Biogeocenol, Inst Soil Science & Agrochem, Russian Acad Sci, Siberian Branch,*

13 *Novosibirsk, Russia*

⁵ N. Laverov Federal Center for Integrated Arctic Research, Russian Academy of Sciences, Arkhangelsk, Russia

17 *Email: oleg.pokrovsky@get.omp.eu

19 Key words: *mercury, peat soil, landscape, bog, forest, thaw, Siberia*

27

28 **Abstract**

29 Natural and anthropogenic mercury (Hg) emissions are sequestered in terrestrial soils over short,
30 annual, to long, millennial time scales, before Hg mobilization and run-off impacts wetland and
31 coastal ocean ecosystems. Recent studies have used Hg to carbon (C) ratios, R_{HgC} , measured in
32 Alaskan permafrost mineral and peat soils, together with a northern circumpolar permafrost soil
33 carbon inventory, to estimate that these soils contain large amounts, 184 to 755 Gg of Hg in the
34 upper 1 m. However, measurements of R_{HgC} on Siberian permafrost peatlands are largely
35 missing, leaving the size of estimated northern soil Hg budget, and its fate under Arctic warming
36 scenarios uncertain. Here we present Hg and carbon data for 6 peat cores, down to mineral
37 horizons at 1.5 - 4 m depth, across a 1700 km latitudinal (56 to 67°N) permafrost gradient in the
38 western Siberian lowlands (WSL). Mercury concentrations increase from south to north in all
39 soil horizons, reflecting a higher stability of sequestered Hg with respect to re-emission. The
40 R_{HgC} in the WSL peat horizons decreases with depth from 0.38 Gg Pg⁻¹ in the active layer to
41 0.23 Gg Pg⁻¹ in continuously frozen peat of the WSL. We estimate the Hg pool (0-1 m) in the
42 permafrost-affected part of the WSL peatlands to be 9.3 ± 2.7 Gg. We review and estimate pan-
43 arctic organic and mineral soil R_{HgC} to be 0.19 and 0.63 Gg Pg⁻¹, and use a soil carbon budget
44 to revise the pan-Arctic permafrost soil Hg pool to be 72 Gg (39-91 Gg, interquartile range
45 (IQR)) in the upper 30 cm, 240 Gg (110-336 Gg) in the upper 1 m, and 597 Gg (384-750 Gg)
46 in the upper 3 m. Using the same R_{HgC} approach, we revise the global upper 30 cm soil Hg pool
47 to contain 1086 Gg of Hg (852-1265 Gg, IQR), of which 6% (72 Gg) resides in northern
48 permafrost soils. Additional soil and river studies in Eastern and Northern Siberia are needed to
49 lower the uncertainty on these estimates, and assess the timing of Hg release to atmosphere and
50 rivers.

51

52

53 **1. Introduction**

54 High-latitude organic-rich soils are key ecosystems controlling the transfer of carbon,
55 nutrients, and pollutants between the atmosphere, rivers, lakes and the Arctic Ocean. These soils
56 are most vulnerable to on-going climate change, due to the high potential mobility of carbon stored
57 in the form of peat deposits. Part of the peat layers are currently frozen but may be subjected to
58 fast thawing, especially in discontinuous and sporadic permafrost zones (Romanovsky et al.,
59 2010). Whilst the stock of C in Arctic and subarctic peat and mineral soils is fairly well quantified
60 (472 Pg C (± 27 Pg, 95% confidence interval, CI) in the upper 0-1m (Hugelius et al. 2014), this is
61 not true for pollutants such as mercury (Hg). Because of its strong bio-amplification in Arctic
62 marine biota (Morel et al., 1998), and exposure to native Arctic populations (AMAP, 2011), there
63 is a strong interest in understanding Hg biogeochemistry in Arctic environments (Outridge et al.,
64 2008; Steffen et al., 2008; Stern et al., 2012).

65 Recent advances in quantifying Arctic Hg cycling show that Arctic Hg^{II} wet deposition is
66 generally low (Pearson et al., 2019), and that the vegetation Hg pump drives yearlong net gaseous
67 Hg⁰ (and CO₂) deposition, via foliar uptake to Arctic vegetation and litterfall to soils (Obrist et al.
68 2017; Jiskra et al., 2018, 2019). Soil core analyses in Alaska indicate that large amounts of carbon
69 and Hg have accumulated since the last glacial maximum (Olson et al., 2018; Schuster et al.,
70 2018). Two upscaling approaches reported differing estimates for the 0 to 1 m soil pool of the
71 northern circumpolar permafrost region of 184 Gg (Olson et al., 2018) and 755 Gg (Schuster et
72 al., 2018).

73 Despite the overall net atmospheric Hg deposition to soils, research has found that Arctic rivers
74 export 37 to 44 Mg y⁻¹ of soil Hg, bound to particulate and dissolved organic matter, to the Arctic
75 Ocean (Fisher et al., 2012; Dastoor et al., 2014; Zhang et al., 2015; Sonke et al., 2018; Zolkos et
76 al., 2020). Together with coastal erosion of soils (30 Mg y⁻¹), river Hg inputs constitute a terrestrial
77 Hg flux of 74 Mg y⁻¹ to the Arctic Ocean that is of similar magnitude to gross atmospheric

78 deposition (80 Mg y⁻¹) over the Arctic Ocean (Sonke et al., 2018). Permafrost thawing has been
79 shown to enhance river Hg export from soils to rivers (St Pierre et al., 2018). It is most pronounced
80 in the discontinuous permafrost zone due to thawing of fresh soil organic matter and maximal
81 active layer depth, and has been suggested to potentially double over the next 50 years (Lim et al.,
82 2019). The quantity of atmospheric Hg deposition to northern peat soils that is presently re-emitted
83 to the atmosphere is not well understood. Hg exchange studies indicate temporally limited Hg⁰
84 emission from the Alaskan permafrost tundra at 68°N (Obrist et al., 2017), and year round net Hg⁰
85 emission from Scandinavian peat at 64°N (Osterwalder et al., 2018). Other studies provide
86 evidence for vegetation type (Rydberg et al., 2010) and temperature and insolation control
87 (Fahnestock et al., 2019) on net Hg⁰ deposition or emission.

88 All available data of Hg in permafrost soils originate from N-America or Scandinavia
89 (Jensen et al., 1991; Bailey et al., 2002; Talbot et al., 2017; Schuster et al., 2018; Olson et al.,
90 2018). Except for three studies (Golovatskaya et al., 2009; Lyapina et al., 2009; Vasilevich, 2018),
91 we did not find extensive measurements of Hg in peat profiles from boreal and permafrost regions
92 of the Russian Arctic and Siberia. Recent work used a soil carbon model to estimate the size of
93 the northern permafrost soil Hg inventory to be 755 ± 427 Gg (95% CI) in the upper 1 m (Schuster
94 et al., 2018). However, this estimate is based on extrapolation of high Hg to organic carbon (C)
95 ratios, R_{HgC} , of 1.6 Gg Hg per Pg of C (Gg Pg⁻¹) in Alaskan mineral soils to the entire North
96 American and Eurasian permafrost zone. Another study used lower R_{HgC} , of 0.12 to 0.62 Gg Pg⁻¹,
97 derived from observations on both Alaskan organic and mineral soils and literature data, to
98 estimate a lower northern soil 0-1 m Hg inventory of 184 Gg (136-274 Gg, 37.5-62.5 percentiles)
99 (Olson et al., 2018). Both studies provide the Hg inventory by multiplying the respective R_{HgC}
100 with the same C pool estimates for the northern circumpolar permafrost region, covering an area
101 of 17.8×10^6 km² (Hugelius et al., 2014).

102 Direct measurement of soil Hg and carbon profiles in frozen peatlands of Siberia are
103 needed to address these variable R_{HgC} and Hg pool estimates of pan-Arctic permafrost soils. This
104 constitutes the first and main objective of the present study. The second objective was assessing
105 the impact of permafrost type (absent, sporadic, discontinuous and continuous) on Hg
106 concentrations and pools in the active layer, frozen peat and mineral horizons. The third objective
107 was to relate Hg concentration in peat to that of other trace metals in order to reveal possible
108 mechanisms of Hg and other metal pollutant accumulation within the organic and mineral horizons
109 of frozen peatlands. Finally, we revisit the world soil Hg inventory in order to put the pan-Arctic
110 permafrost soil Hg pool into global perspective.

111

112 2. Study Site and Methods

113 2.1. Sampling sites

114 Soil sampling was performed along a latitudinal transect of the western Siberia lowlands
115 (WSL) that comprised the southern taiga (Plotnikovo, 56°N), the middle taiga (Mukhrino, 60°N),
116 the northern part of the taiga zone (Kogalym, 62°N), forest-tundra (Khanymey 62°N and Pangody,
117 65°N) and tundra (Tazovsky, 67°N) biomes (Fig. 1). In the WSL, the permafrost zones follow the
118 temperature and vegetation distribution over the latitude at otherwise similar relief, lithology and
119 runoff, thus allowing to test the effect of permafrost by analyzing latitudinal features of Hg
120 distribution in soils. Key physico-geographical parameters of studied sites and soil types are listed
121 in Table S1. The WSL peat actively formed since the beginning of the Holocene until freezing of
122 bogs in the sub-Boreal period (11-4.5 ky, Kremenetski et al., 2003; Panova et al., 2010;
123 Ponomareva et al., 2012; Loiko et al., 2019). Since 4.5 ky, the rate of peat formation and bog
124 extension in the permafrost-affected part of the WSL have decreased. In the southern part of
125 cryolithozone and permafrost-free part of WSL, peat accumulation and bog extension remained
126 active over the entire Holocene (Kurina and Veretennikova, 2015; Preis and Karpenko, 2015;

127 Kurina et al., 2018). The main mineral substrates underlying frozen peat layers of the WSL are
128 quaternary clays, sands, and alevrolites. In the southern part (sites Plotnikovo and Mukhrino), the
129 typical substrate is carbonate-bearing clays of lake-alluvium origin with rare layers of sandstones
130 (**Table S1**).

131 Mean annual **ambient** temperature (MAAT) **decreases** from south to north, being equal to
132 $-0.4, -1.2, -4.0, -5.6, -6.4$, and -9.1°C at Plotnikovo, Mukhrino, Kogalym, Khanymey, Pandogy
133 and Tazovsky, respectively (Trofimova and Balybina, 2014). The permafrost is absent in
134 Plotnikovo but present at all other sites and ranges from relict to isolated (Mukhrino) **and** isolated
135 to sporadic (Kogalym) in the south, to discontinuous (Khanymey, Pangody) and continuous
136 (Tazovsky) in the north. At permafrost-affected sites, the average active layer thickness (ALT) at
137 the time of sampling of peat mounds (hummocks) ranged from 90 cm in the south to 45 cm in the
138 north. The peat mounds of ombrotrophic bogs probed in this work are present across the full
139 latitudinal gradient.

140 The vegetation of three studied types of bogs (polygonal, flat-mound and ridge-hollow) is
141 essentially oligotrophic (poor in nutrients) which indicates the ombrotrophic (rain and snow water
142 fed) conditions, i.e., the lack of groundwater input and lateral surface influx of nutrients. The flat-
143 mound palsa is covered by dwarf shrubs (*Ledum decumbens*, *Betula nana*, *Andromeda polifolia*,
144 *Vaccinium* ssp., *Empetrum nigrum*), lichens (*Cladonia* ssp., *Cetraria*, *Ochrolechia*) and mosses
145 (*Dicranum* ssp., *Polytrichum* ssp., *Sphagnum angustifolium*, *S. lenense*). At southern sites, the
146 pine *Pinus sylvestris* is abundant on ridges (Peregon et al., 2008, 2009) whereas the two taiga sites
147 are dominated by *Pinus sylvestris* with minor but permanently present *Betula pubescens* and *Pinus*
148 *sibirica*. Dwarf shrubs are dominated by *Ledum palustre*, *Chamaedaphne calyculata*, *Vaccinium*
149 *vitis-idaea*. The moss layer is dominated by ***S. fuscum***, *S. angustifolium* with the presence of ***S.***
150 *magellanicum*, *S. capillifolium* and boreal forest moss species like *Pleurozium schreberi*.

151

152 2.2. *Sampling procedure, analyses and data treatment*

153 Peat core samples were collected in August, when the depth of unfrozen layer was at its
154 maximum (i.e., see Raudina et al., 2017). Based on measurements by temperature loggers over
155 the summer period, the in-situ temperature of studied soil profile ranged from $15\pm5^{\circ}\text{C}$ in the top
156 soil (0-20 cm) to $4\pm2^{\circ}\text{C}$ at the permafrost boundary (40-80 cm). **Field logistics and financial**
157 **resources did not make it possible to study multiple cores from each climate zone.** The physical,
158 chemical and botanical properties of several peat cores collected in the homogeneous palsa region
159 in the north and ridge-ryam complex in the south are highly similar among different peat mounds,
160 **suggesting that the cores we obtained are representative for the** WSL (Velichko et al., 2011;
161 Stepanova et al., 2015).

162 Peat cores were extracted using a Russian sediment/peat corer and the frozen part was
163 sampled using a motorized Russian peat corer (UKB-12/25 I, Russia) with a 4-cm diameter corer
164 sterilized with 40% ethanol prior to each extraction. We collected the full active (unfrozen) layer
165 peat column, the frozen peat column and some 10 to 30 cm of frozen mineral horizons using clean
166 powder-free vinyl gloves. Peat or mineral soil samples were divided in 5-10 cm segments using a
167 sharp sterile single-use plastic knife. Soil samples were placed in sterile PVC doubled-zipped bags
168 and kept at -20°C during transport and storage. To avoid contamination of peat from external
169 surroundings, we separated the part of the core for geochemical analysis exclusively from the
170 interior of the core (> 1 cm from the core liner) following conventional procedures (Wilhelm et
171 al., 2011).

172 Total Hg concentration, THg, in freeze-dried and ground slices of peat cores was
173 determined using a direct mercury analyzer (DMA-80 - Milestone, Italy). Analysis of reference
174 material BCR-482 (lichen, $480\pm28 \text{ ng g}^{-1}$), MESS-3 (sediment, $91\pm9 \text{ ng g}^{-1}$) and NIST **SRM** 1632d
175 (coal, $93\pm3 \text{ ng g}^{-1}$) showed good reproducibility (mean $\pm 1\sigma$) of $467\pm28 \text{ ng g}^{-1}$, $80\pm6 \text{ ng g}^{-1}$ and
176 $98\pm8 \text{ ng g}^{-1}$, respectively. The average uncertainty on duplicate sample analysis did not exceed

177 5% (1σ). The carbon (C) and nitrogen (N) concentration were measured using catalytic
178 combustion with Cu-O at 900°C with an uncertainty of $\leq 0.5\%$ using Thermo Flash 2000 CN
179 Analyzer, and aspartic acid (C 36.1% $\pm 1.5\%$; N 10.5% $\pm 0.5\%$) and soil reference material (C
180 2.29% $\pm 0.07\%$; N 0.21% $\pm 0.01\%$) as standards. Analyses of total C before and after sample
181 treatment with HCl did not yield more than 1 % of inorganic C; therefore our total C-determination
182 represents organic carbon. For trace and major element analysis, soil samples were subjected to
183 full acid digestion in the clean room following ICP-MS (inductively coupled plasma mass
184 spectrometry, Agilent 7500 ce) analyses as described previously (Morgalev et al., 2017).

185 The Shapiro Wilk normality test was used to asses THg, elemental and R_{HgC} distributions,
186 and statistical data descriptors adjusted accordingly. All statistical tests used a significance level
187 of 95% ($\alpha = 0.05$). Spearman rank order correlations (significant at $p < 0.05$) were performed to
188 characterize the link of Hg with C, N and other major and trace elements. The differences in Hg
189 concentration between the active- and frozen peat layer were tested using the Mann-Whitney U
190 test for paired data at a significance level of 0.05.

191 C pools of different soil classes reported by Hugelius et al. (2014) were divided into two
192 categories, organic and mineral soils. Histosols and Histels were defined as organic soils. Turbels
193 and Orthels were considered as organic soils for the 0 – 0.3 m interval and as mineral soils for the
194 0.3 – 3m interval. All other soils were considered as mineral soils. To estimate the pan-Arctic
195 permafrost soil Hg pool, C pools were multiplied with the respective R_{HgC} derived for organic
196 (>20% C) and mineral (<20% C) soil data from Eurasia and North America (excluding Alaska).
197 To calculate the global Hg pool, a simpler approach was used and one single R_{HgC} was considered
198 for 5 climate zones which were defined by latitude (arctic: $> 67^\circ$, boreal: 50° - 67° , temperate:
199 35° - 50° , subtropical: 23.45° - 35° , tropical: $< 23.45^\circ$) according to FAO and ITPS (2018). The
200 uncertainty was assessed with a Monte carlo approach using the *rnorm* and *rlnorm* function of R
201 (version 3.6.1.) and is reported as the interquartile range (25th and 75th percentile) of 100,000

202 simulations. For the pan-Arctic permafrost soil Hg pool, final uncertainties incorporate the
203 uncertainties on the C stock from Hugelius et al. (2014) assuming normal distribution and
204 uncertainties of R_{HgC} assuming log-normal distribution.

205

206 **3. Results**

207 *3.1. Depth (vertical) distribution of Hg in WSL peat profiles*

208 Hg concentration in peat cores of the WSL are illustrated in **Fig. 2** and primary data on
209 soil chemical composition and Hg concentration are listed in **Table S2** of the Supplement. The
210 upper 0-20 cm layer is 2 to 3 times enriched in Hg compared to the rest of the peat core in
211 permafrost-affected sites (Khanymey, Pangody and Tazovsky). This is not the case, however, for
212 the sporadic permafrost zone (Kogalym) and isolated permafrost zone (Mukhrino), where a local
213 maximum at ca. 35 cm depth was detected but no enrichment of upper 10-20 cm horizons
214 occurred. In the most southern, permafrost-free site of the WSL (Plotnikovo, southern taiga), the
215 Hg concentration profile in the peat was fairly constant with a local minimum at 100 cm depth.
216 The mean, depth-integrated Hg concentrations in active layer, permafrost and mineral horizons
217 are illustrated in **Fig. 3** and summarized in **Table 1**. The latitudinal trend of Hg concentration in
218 peat consists of a systematic increase northward, both in permafrost and active peat layers. The
219 dominant ground vegetation (lichens) analyzed at 5 sites out of 6 (Plotnikovo, Kogalym,
220 Khanymey, Pangody and Tazovsky) did not show significantly different (U test Mann-Whitney)
221 Hg concentrations relative to the peat cores (**Fig. 3**). Mercury concentrations in the six WSL peat
222 cores ranged from 7 to 284 ng g⁻¹ with a median (\pm IQR) of 67 \pm 57 ng g⁻¹. The Hg concentration
223 in the thawed, active layer was generally comparable to that in the frozen layer, supported by a
224 Mann-Whitney test, which did not show significant difference in Hg concentration between frozen
225 and thawed peat in all permafrost-affected sites. Within the latitudinal transect from south to north,

226 the Hg concentrations in peat are higher (Plotnikovo, Kogalym, Khanymey, Pangody) or
227 comparable (Tazovsky) to those in the mineral horizons.

228 The ratio of Hg:C (R_{HgC} , $\mu\text{g g}^{-1}$, corresponding to Gg Pg^{-1}) ranged between 0.05 and 2.0
229 over the peat columns, and was 5 to 10 times higher in mineral horizons compared to frozen peat
230 and active layers (**Fig. 4**). The R_{HgC} in the active layer and in the mineral horizons increased 3-
231 fold from the south (56°N) to the north (67°N). In the frozen peat horizon, the R_{HgC} ratio increased
232 two-fold from sporadic and isolated to continuous permafrost zone.

233

234 *3.2. Regional and total pools of Hg in the WSL peat and mineral layers*

235 The mass of Hg per area of soil in the active- and frozen peat layer as well as in the top 30
236 cm of frozen mineral horizons of the six studied WSL peat profiles was calculated by multiplying
237 bulk soil peat and mineral layer densities (range from 0.01 to 0.38 g/cm^3 , **Table S2**) by Hg
238 concentration and integrating over the corresponding depths. The surface area - normalized Hg
239 stock systematically increased from south to north (ca. 0.3 to 6.0 mg Hg m^{-2} and ca. 0.8 to 13.7
240 mg Hg m^{-2} , in the 0-30 and the 0-100 cm peat layer, respectively (**Fig. 5 A**). This northward
241 increase was most pronounced for the active layer, was less evident for frozen peat, and
242 insignificant for the upper 30 cm of mineral horizon located under the peat (**Fig. 5 B**). Taking into
243 account the proportion of bogs (peatlands) in each zone (1° latitudinal grid) from Sheng et al.
244 (2004), we calculated the pool of Hg in permafrost-free and permafrost-affected WSL peatlands
245 (**Fig. 6**). The total pool of Hg in the 0-100 cm layer of peat bogs exhibits a maximum (356-580
246 Mg) in the discontinuous permafrost zone.

247 We estimate the total organic soil Hg pool in the WSL from the Hg stock (mg Hg m^{-2} over
248 0-100 cm depth) for permafrost and permafrost-free zones (**Fig. 7 A**), extrapolated to the full
249 average thickness of peat in the WSL (280 cm, Sheng et al., 2004), assuming that Hg concentration
250 in the upper 0-100 cm peat layer is the same as in 100-280 cm of peat and multiplied by the area

251 of bogs in each latitudinal grid (S, m²) as shown in **Fig 7 B**. This yields 1.7 Gg Hg in the
252 permafrost-free zone and 7.6 Gg Hg in the permafrost-bearing zone with a total Hg pool of 9.3
253 Gg in the WSL. For this calculation we did not take into account the mineral horizons and we used
254 variable active layer thickness across the latitudinal gradient of WSL, as estimated at our sampling
255 sites (**Table S1**). The amount of Hg in permafrost-bearing zone within the active (unfrozen) peat
256 layer (0-160 cm in the south and 0-20 cm in the north) of the WSL is 2.0 Gg, and that in the frozen
257 (160-280 cm in the south and 20-280 cm in the north) layer is 5.6 Gg.

258 Alternatively, to calculate the total pool of Hg in WSL bogs, we used the R_{HgC} inferred
259 from our data across the gradient of permafrost and biomes (Table 1). Taking into account the C
260 pool in the WSL (70.2 Pg C of 0-280 cm depth layer, Sheng et al., 2004) and the median R_{HgC} of
261 0.133 Gg Pg⁻¹ in the WSL, we calculated Hg for the full depth of the peat layer in each zone. This
262 also gives 9.3 Gg Hg for a total area of 592,440 km².

263

264 *3.3. Correlation of Hg with other elements in the peat cores*

265 Spearman rank order correlations of Hg with other elements demonstrated significant
266 positive relationships ($R > 0.60$; $p < 0.05$) with K, Rb, Cs, P, As, W, V, Cr, Cu in the active
267 (unfrozen) layer (**Table S3** of Suppl). However, these relationships were less pronounced in
268 the frozen peat, where only Mg, Ca, Sr, Mn, N, P, As, Cu, Ni, Sb and some REE demonstrated
269 minor ($0.40 < R < 0.55$) positive correlations with Hg. Finally, in the mineral layer, significant
270 ($R > 0.70$) positive correlations of Hg were observed with Li, Ca, Sr, P, N, Mn, Ni, Co, Cr, Cd. A
271 positive ($R = 0.60$) relationship between Hg and C was observed in mineral horizons, whereas no
272 correlation was detected in both frozen and thawed peat. This is consistent with some studies of
273 peat soil in Brazil (Roulet et al., 1998) and Arctic tundra soils (Olson et al., 2018). At the same
274 time, there was a positive correlation of Hg with nitrogen (N) in the active layer, frozen peat and

275 mineral horizons ($R = 0.50, 0.47$ and 0.75 , respectively). Stronger and more stable correlation of
276 Hg with N compared to C was also noted by Roulet (2000).

277

278 **4. Discussion**

279 *4.1. Hg association with other elements in peat*

280 Stronger accumulation of Hg relative to C in mineral horizons in the north (Tazovsky, **Fig.**
281 **4**) may be linked to the clay nature of mineral layers (Roulet et al., 1998; Baptista-Salazar et al.,
282 2017) in these regions (**Table S1**), but also to the presence of specific host phases of Hg (see
283 examples of peat minerals in Rudmin et al., 2018). Dissolved oxygen measurements in soil
284 porewaters at the Tazovsky site indicate that mineral gleysoils and peat histosols, which often
285 overlay former lake sediments, are anoxic (Raudina et al., 2017; Loiko et al., 2019). The Hg host
286 phases in these soils are therefore likely sulfide minerals. Indeed, known Hg carriers in peat
287 deposits are Fe and Zn sulfide minerals or organic-bound sulfide functional groups (Smieja-Król
288 et al., 2010; 2014; Prietzel et al., 2009; Skyllberg et al., 2003, Bates et al., 1998; Steinmann and
289 Shotyk, 1997).

290 In the peat active layer, Hg was positively correlated with K, Rb, Cs, P, As, V, Cr, Cu
291 (**Table S3**). In the frozen part of the peat core, Hg was positively correlated with Ca, N, Mn, Sr,
292 Mg, P (**Table S3**). Indeed, atmospheric particles in snow across the WSL exhibit strong
293 enrichment in Mo, W, As, Sb, Ni, Cu, Zn, Cd, Pb, Mg, Ca, and Na (Shevchenko et al., 2017). The
294 strong positive correlation of Hg with these elements in peat soils of WSL suggests a common
295 atmospheric origin. Note however, that the cited elements deposit with particles, rainfall and
296 snowfall, whereas atmospheric Hg transfer to peat occurs mainly via the vegetation pump, with
297 tundra and taiga vegetation actively taking up atmospheric gaseous Hg^0 through foliage (Obrist
298 et al., 2017; Jiskra et al., 2018).

299

300 4.2. *Estimating the pan-Arctic permafrost soil Hg pool*

301 A recent study used a median R_{HgC} value of 1.6 Gg Pg^{-1} , observed mainly in mineral soil
302 samples (median SOC of 3%, IQR=1.7 to 8.7 %) along a transect in Alaska, to estimate a pan-
303 Arctic permafrost soil Hg pool of $755 \pm 427 \text{ Gg}$ in the upper 0-100 cm, and $1656 \pm 962 \text{ Gg}$ in the
304 upper 0-300 cm (Schuster et al. 2018). In the case of western Siberia, this high R_{HgC} value
305 overestimates the Hg pool 12-fold, given that the median R_{HgC} in WSL peat is only $0.13 \pm 0.12 \text{ Gg}$
306 Pg^{-1} (median±IQR) (**Table 1**, **Fig. 4**). The extrapolation based on Alaskan R_{HgC} for the whole
307 Northern Hemisphere permafrost region also suggests that the WSL contains large amounts of Hg
308 in the upper 0-30 cm ($20\text{-}40 \text{ mg Hg m}^{-2}$) and in the upper 0-100 cm ($40\text{-}80 \text{ mg Hg m}^{-2}$). These
309 numbers are much higher than the direct measurements in this study: 0.3 mg Hg m^{-2} in 0-30 cm
310 and $0.8\text{-}1.3 \text{ mg Hg m}^{-2}$ in 0-100 cm layer in the permafrost-free zone (Plotnikovo and Mukhrino
311 sites); 0.5 mg Hg m^{-2} in 0-30 cm and 3.0 mg Hg m^{-2} in 0-100 cm layer in the sporadic zone
312 (Kogalym site); $1.8\text{-}4.0 \text{ mg Hg m}^{-2}$ in 0-30 cm and $9.6\text{-}11.9 \text{ mg Hg m}^{-2}$ in 0-100 cm layer in the
313 continuous to discontinuous permafrost zone (Khanymey and Pangody sites), and 6.0 mg Hg m^{-2}
314 in 0-30 cm and $13.7 \text{ mg Hg m}^{-2}$ in 0-100 cm layer in continuous permafrost zone (Tazovsky). It
315 is worth noting that the recent data of Talbot et al. (2017) for Ontario (Canada) bogs ($S_{\text{area}} =$
316 $1,133,990 \text{ km}^2$; 18.8 Gg Hg for the $277 \pm 123 \text{ cm}$ depth) are consistent with the results of the
317 present study in the WSL (9.3 Gg Hg for $592,440 \text{ km}^2$ for the $280 \pm 100 \text{ cm}$ depth).

318 A revised value of the Hg pool in the pan-Arctic permafrost soils was recently provided
319 by Olson et al. (2018) who combined measured R_{HgC} values for Alaskan tundra soils (**Dalton**
320 **Highway, Noatak National Preserve, 8 Mile Lake Observatory**) with literature data (**Table S4**),
321 and derived R_{HgC} of 0.12 Gg Pg^{-1} for 0-30 cm (organic) and 0.62 Gg Pg^{-1} for 30-100 cm (mineral)
322 layers. Note that Olson et al. Table 1 has an incorrect organic soil R_{HgC} of 0.274 Gg Pg^{-1} , which
323 should be 0.119 Gg Pg^{-1} ; the typo did not affect their soil Hg budgets. Olson et al. (2018) estimate
324 pan-Arctic permafrost soil Hg pools of 26 Gg (0-30 cm) and 158 Gg (30-100 cm), which combined

325 (184 Gg) is 4 times lower than the number of 755 Gg (0-100 cm) by Schuster et al. (2014). Both
326 studies report R_{HgC} measurements from Alaskan soils, due to relatively easy road access to the
327 sampling sites along the Dalton Highway. The bedrock along the Dalton Highway contains
328 relatively high geogenic Hg levels (mean concentration: 32 ng/g), resulting in a high geogenic
329 contribution in mineral soils (39% for B horizons and 20% for A horizons, Obrist et al., 2017). It
330 is clear that any upscaling calculation of pan-Arctic permafrost Hg depends critically on the R_{HgC}
331 of the 0-30 and 30-100 cm peat layers, as Eurasian sporadic to continuous permafrost represents
332 54% of the northern soil C inventory (Table 2). We combined our new WSL data (n=202) with
333 literature data covering Russia (n=42), Scandinavia (n=97), Canada (n=122) and Alaska (n=703)
334 to build a pan-arctic database for RHgC (Table S4). Setting Alaska aside, as a geographic region
335 with high geogenic Hg, we find that Eurasian and North American (excluding Alaska) mineral
336 (<20% SOC) soil R_{HgC} was lower ($\mu = 0.67 \text{ Gg Pg}^{-1}$, median= 0.64 Gg Pg⁻¹ (IQR = 0.33 to 0.79
337 Gg Pg⁻¹), n=130) than R_{HgC} reported for mineral soils along the Dalton highway in Alaska
338 (median= 1.64 Gg Pg⁻¹ (IQR = 0.91 to 2.93 Gg Pg⁻¹), n=589) (Schuster et al., 2018) (Figure 8).
339 The R_{HgC} in organic soils (>20% SOC, including data from Alaska) was approximately 4 times
340 lower ($\mu = 0.19 \text{ Gg Pg}^{-1}$, median= 0.15 Gg Pg⁻¹ (IQR = 0.09 to 0.25 Gg Pg⁻¹), n=446) than that in
341 mineral soils of Eurasia and North America (excluding Alaska) (Figure 8), consistent with the
342 observed difference in WSL mineral and organic soils. Higher R_{HgC} observed in mineral soils may
343 originate from a contribution of geogenic Hg from the weathered bedrock (independent of C stock)
344 and/or a higher mineralization rate of C (preferential C over Hg loss) in predominantly oxic
345 mineral soils compared to anoxic peat soils.

346 In Table 2 we revisit the full 0-300 cm pan-Arctic permafrost soil Hg inventory. For this,
347 we used Eurasian and North-American (excluding Alaska) R_{HgC} based on the literature data
348 compilations of Olson et al. (2018) and Schuster et al. (2018), and our observed WSL R_{HgC} for
349 Eurasia, multiplied by estimated organic C pools for the northern permafrost region covering 17.8

350 $\times 10^6 \text{ km}^2$ from Hugelius et al. (2014). The systematic underestimation made by neglecting high
351 R_{HgC} in Alaskan mineral soils is small, on the order of 2.5 Gg Hg, due to relatively small Alaskan
352 C pool of 2.6 Pg C (Tarnocai et al., 2009). We estimate the pan-Arctic permafrost soil Hg pool to
353 be 72 Gg (39-91 Gg, IQR) in the upper 30 cm, 240 Gg (110-336 Gg) in the upper 1 m, and 597
354 Gg (384-750 Gg) in the upper 3 m (Table 3). Note that our revised value in the 0 - 1m range (240
355 Gg) is similar to that of Olson et al. (184 Gg), but sizably lower than that of Schuster et al. (755
356 Gg). We find that Hg stocks in organic soils (>20% SOC) represent 52% and 21% of the total Hg
357 stock in the 0-30 cm and 0-100 cm depth range, respectively (Table 2). The rest of the pan-arctic
358 Hg is associated with C in mineral soils (<20% SOC) for which relatively sparse data exists
359 (n=131). In particular, turbel and orthel mineral soils, which are estimated to contain 49 to 62%
360 of total arctic C (Hugelius et al., 2014) and 36 to 85% of Hg at the various depth intervals need to
361 be further investigated.

362

363 4.3. Estimating Earth's global soil (0-30 cm) Hg pool

364 To assess Earth's global soil Hg pool, we combined the more detailed Arctic pool estimate
365 (separating organic and mineral soils) with a more basic approach for the other climate zones,
366 where we derived bulk R_{HgC} for the 0-30 cm surface soils based on published literature data. Core
367 dataset for this analysis was the global literature compilation by Schuster et al. 2018 with 11,000
368 datapoints, of which 6,224 datapoints were from 0-30 cm range. This global dataset was
369 complemented by soil Hg data from the boreal (Olson et al., 2018) and tropical (Campbell et al.,
370 2003; Almeida, 2005; Almeida et al. 2005; Melendez-Perez et al., 2014) zone. The R_{HgC} for each
371 climate zone (arctic, boreal, temperate, subtropical and tropical) were then multiplied with the
372 respective C stock estimates from the global soil organic carbon map (FAO and ITPS, 2018). The
373 R_{HgC} of all 0 to 30 cm soil data increases from cold climate zones to warmer climate, from 0.36
374 Gg Pg⁻¹ for Arctic soils (excluding Alaska), to 1.8 Gg Pg⁻¹ in subtropical and tropical soils (Figure

375 **9, Table 4).** This latitudinal trend in R_{HgC} likely reflects a combination of low C mineralization
376 rates in colder north and additional Hg sorption to Fe(oxi)hydroxides in old tropical soils. Taking
377 into account the variation in R_{HgC} and C stocks across the climate zones, we estimate a global Hg
378 stock of 1086 Gg (852 – 1265 Gg, IQR) for the top 0 - 30 cm (**Table 4**). Previous global Hg soil
379 pool estimates vary between 232 and 1150 Gg (Selin et al., 2008; Smith-Downey et al., 2010;
380 Amos et al., 2013, 2015; Hararuk et al., 2013; Wang et al., 2019). Schuster et al. (2018) concluded
381 that Arctic permafrost soils store nearly twice the amount of Hg as all other soils, the ocean and
382 atmosphere combined, but in doing so they compared different depth ranges for global (typically
383 0-15 cm or 0-20 cm) and Arctic soil estimates (0 - 300 cm). Our revised estimate of the pan-Arctic
384 permafrost and global soil pool suggests that, for a similar depth range of 0-30 cm, permafrost
385 soils contain 6% (72 Gg) of the global soil Hg pool (1086 Gg).

386

387 *4.4. Northern soil Hg sequestration and Hg loss*

388 Olson et al. (2018) recognized that the large 0-100 cm northern soil Hg pool is the result
389 of thousands of years of net atmospheric Hg deposition. The latitudinal trend of northward
390 increasing peat Hg concentration in the WSL (**Fig. 4, 5**) illustrates that this net Hg deposition is a
391 fine balance between the vegetation Hg pump, which sequesters Hg^0 in soils via foliar uptake and
392 litterfall, and Hg^0 emission during biomass degradation. Annual gross Hg sequestration by
393 vegetation, via the vegetation pump, likely scales with primary productivity and therefore
394 decreases northward as insolation and growing season decrease. However, in the north,
395 degradation rates of vegetation biomass are lower than in the south: the moss biomass losses
396 during decomposition in the forest tundra zone (5-6% over 1st year and 10-12% over 2 years) is
397 lower than that in the southern taiga (10-20% over 1st year and 20-40% over 2 years), based on in-
398 situ biomass degradation experiments across the WSL gradient of biomes (Vishnyakova and
399 Mironycheva-Tokareva, 2018). The net result is a higher preservation of soil Hg in the north,

400 where less emission of Hg^0 during plant decay occurs. The dependence of this balance, between
401 Hg^0 sequestration and Hg^0 re-emission, on climate explains qualitatively the contrasting
402 observations made in Toolik (AK, USA, 68°N , MAAT = -7°C , Obrist et al., 2017) and Degerö
403 Stormyr (Sweden, 64°N , MAAT = 2°C , Osterwalder et al., 2018). At Toolik, net Hg^0 deposition
404 by vegetation and soil uptake occurs on an annual basis, whereas at Degerö Stormyr higher
405 temperatures result in net annual Hg^0 emission. More research is needed to quantify the climate
406 dependence of Hg^0 sequestration (as soil Hg^{II}) and Hg^0 re-emission before we can predict and
407 model northern soil Hg loss to the atmosphere due to global warming trajectories.

408
409 **5. Conclusions**

410 Western Siberian peatlands contain a large amount of Hg in frozen and thawed peat; the
411 lateral pools of peat palsas range from $1\text{-}2 \text{ mg Hg m}^{-2}$ in the south to $10\text{-}15 \text{ mg Hg m}^{-2}$ in the
412 north. This northward increase of Hg concentration and pools can be explained by better
413 preservation of organic-bound Hg, **i.e. lower Hg re-emissions**, due to colder temperatures and
414 shorter active period in the continuous permafrost zone compared to the discontinuous and
415 sporadic zones. We revisited the full 0-300 cm **pan-Arctic** permafrost soil Hg inventory, based on
416 published R_{HgC} and our observed WSL R_{HgC} , together with estimated **pan-Arctic permafrost** soil
417 organic C pools for 0-300 cm from Hugelius et al. (2014). We estimate the 0-300 cm **pan-Arctic**
418 permafrost soil Hg inventory to be **597 Gg** (**384-750 Gg**, IQR), which is three times lower than a
419 previous estimate of $1656 \pm 962 \text{ Gg Hg}$ for the same depth range (Schuster et al., 2018). We
420 estimate the global soil Hg pool to be **1086 Gg** for the 0-30 cm depth range. The permafrost Hg
421 pool for the same 0 - 30 cm depth range is **77 Gg**, and while large compared to the 3 Gg of Hg
422 residing in the Arctic **Ocean** (Soerensen et al., 2016), it represents only **6%** of the global soil Hg
423 **pool**.

424 We document large regional differences in R_{HgC} driven by (1) different contributions of
425 **geogenic Hg in mineral soils**, e.g. resulting in higher R_{HgC} in Alaska than in other areas of the pan-

426 Arctic permafrost region and (2) the stability of Hg with respect to emission from organic soils,
427 e.g. resulting in a gradient with increasing R_{HgC} towards the north of the WSL. These systematic
428 differences illustrate the limitations of the poolsize estimation approach where C inventories are
429 multiplied with average R_{HgC} values and emphasize the need for spatially resolved sampling and
430 pool size estimates, similar to the pan-Arctic permafrost C pool estimates (Hugelius et al., 2014).
431 In particular, to estimate the release of Hg to aquatic ecosystems, e.g. coastal erosion and transfer
432 to rivers, and Hg evasion to the atmosphere, spatially resolved Hg soil pools will be valuable.

433

434 **Data availability.** Hg and C concentration data of the WSL soil samples are available in the
435 supplement. A summary of pan-Arctic literature data is provided in the supplement. The
436 permafrost data from Schuster et al. 2018 and a global compilation of R_{HgC} data is available at
437 (<https://agupubs.onlinelibrary.wiley.com/doi/full/10.1002/2017GL075571>, last access: 6
438 December 2019). The Arctic and boreal soil data from the Olson et al. 2018 study is available
439 from the corresponding author upon request. Note that Olson et al. Table 1 has an incorrect
440 organic soil R_{HgC} of 0.274 Gg Pg^{-1} , which should be 0.119 Gg Pg^{-1} . The data from the tropical
441 climate zone was compiled from original publications of Almeida (2005); Almeida et al. (2005);
442 Campbell et al. (2003); Melendez-Perez et al. (2014).

443

444 **Author contributions.** OSP and SVL designed the study. SVL, AGL, and NK performed field
445 sampling. AGL and OSP did all laboratory analysis. MJ and JES did the northern soil and global
446 soil Hg pool calculations. All authors contributed to writing of the manuscript.

447

448 **We declare no competing interests**

449

450

451 **Acknowledgements:**
452 Fieldwork and data analysis was carried out under support from the Russian Science Foundation
453 (project №18-77-10045). Partial support from the Russian Fund for Basic Research, via grant no.
454 19-29-05209-mk and 19-55-15002-NCNI_a, and from the CNRS Chantier Arctique Français, via
455 the PARCS project, and the H2020 ERA-PLANET (689443) iGOSP and iCUPE programmes are
456 acknowledged. M.J. acknowledges funding by the Swiss National Science Foundation (grant no.
457 PZ00P2_174101). We are thankful to Luiz D. Lacerda for sharing Hg and C data from Brazil.
458

459 **References**
460 Almeida, M. D., Lacerda, L. D., Bastos, W. R., and Herrmann, J. C.: Mercury loss from soils
461 following conversion from forest to pasture in Rondônia, Western Amazon, Brazil, *Environ. Pollut.*,
462 137(2), 179–186, doi:10.1016/j.envpol.2005.02.026, 2005.
463 Almeida, M.D.: Biogeoquímica de mercúrio na interface solo-atmosfera na Amazônia, Ph.D.
464 thesis, Univsidade Federal Fluminense, Niterói, Brazil, 221 pp., 2005.
465 Amos, H. M., Jacob, D. J., Kocman, D., Horowitz, H. M., Zhang, Y., Dutkiewicz, S., Horvat,
466 M., Corbitt, E. S., Krabbenhoft, D. P., and Sunderland, E. M.: Global biogeochemical implications
467 of mercury discharges from rivers and sediment burial, *Environ. Sci. Technol.*, 48(16), 9514–9522,
468 doi:10.1021/es502134t, 2014.
469 Amos, H. M., Sonke, J. E., Obrist, D., Robins, N., Hagan, N., Horowitz, H. M., Mason, R. P.,
470 Witt, M., Hedgecock, I. M., Corbitt, E. S., and Sunderland, E. M.: Observational and modeling
471 constraints on global anthropogenic enrichment of mercury, *Environ. Sci. Technol.*, 49(7), 4036–
472 4047, doi:10.1021/es5058665, 2015.
473 Anisimov, O. A., and Sherstiukov, A. B.: Evaluating the effect of climatic and environmental
474 factors on permafrost in Russia, *Earth's Cryosphere*, XX (2), 78-86, 2016.
475 Anisimov, O., and Reneva, S.: Permafrost and changing climate: the Russian
476 perspective, *AMBIO*, 35(4), 169-176, 2006.
477 Bailey, E. A., Gray, J. E., and Theodorakos, P. M.: Mercury in vegetation and soils at
478 abandoned mercury mines in southwestern Alaska, USA, *Geochemistry Explor. Environ. Anal.*,
479 2(3), 275–285, doi:10.1144/1467-787302-032, 2002.
480 Baptista-Salazar, C., Richard, J. H., Horf, M., Rejc, M., Gosar, M., and Biester, H.: Grain-
481 size dependence of mercury speciation in river suspended matter, sediments and soils in a mercury
482 mining area at varying hydrological conditions, *Appl. Geochemistry*, 81, 132–142,
483 doi:10.1016/j.apgeochem.2017.04.006, 2017.
484 Bates, A. L., Spiker, E. C., and Holmes, C. W.: Speciation and isotopic composition of
485 sedimentary sulfur in the Everglades, Florida, USA, *Chem. Geol.*, 146(3–4), 155–170,
486 doi:10.1016/S0009-2541(98)00008-4, 1998.
487 Bedritsky, A.I.: Global climate and soil cover Russia: estimation of risks and
488 environmental and econoical consequences of land degradation. Adaptive systems and
489 technologies of agriculture and forestry, Moscow, National report, 2018. (In Russian).
490 Brown, J., Ferrians Jr, O. J., Heginbottom, J. A., and Melnikov, E. S.: Circum-arctic map
491 of permafrost and ground ice conditions, National Snow and Ice Data Center, Digital media,
492 Boulder, CO 80309-0449 USA, 1998, revised February 2001.
493 Campbell, L. M., Hecky, R. E., Muggide, R., Dixon, D. G., and Ramlal, P. S.: Variation
494 and distribution of total mercury in water, sediment and soil from northern Lake Victoria, East
495 Africa, *Biogeochemistry*, 65(2), 195–211, doi:10.1023/A:1026058417584, 2003.

496 Dastoor, A. P., and Durnford, D. A.: Arctic Ocean: Is It a Sink or a Source of Atmospheric
497 Mercury?, *Environ. Sci. Technol.*, 48(3), 1707–1717, doi:10.1021/es404473e, 2014.

498 Fahnestock, M. F., Bryce, J. G., McCalley, C. K., Montesdeoca, M., Bai, S., Li, Y.,
499 Driscoll, C. T., Crill, P. M., Rich, V. I., and Varner, R. K.: Mercury reallocation in thawing
500 subarctic peatlands, *Geochemical Perspect. Lett.*, 6, doi:10.7185/geochemlet.1922, 2019.

501 FAO and ITPS: Global Soil Organic Carbon Map (GSOCmap), Technical Report, Rome,
502 162 pp. 2018.

503 Fisher, J. A., Jacob, D. J., Soerensen, A. L., Amos, H. M., Steffen, A., and Sunderland, E.
504 M.: Riverine source of Arctic Ocean mercury inferred from atmospheric observations, *Nat.*
505 *Geosci.*, 5(7), 499–504, doi:10.1038/ngeo1478, 2012.

506 Frey, K. E., McClelland, J. W., Holmes, R. M., and Smith, L. G.: Impacts of climate
507 warming and permafrost thaw on the riverine transport of nitrogen and phosphorus to the Kara
508 Sea, *J. Geophys. Res. Biogeosciences*, 112(4), doi:10.1029/2006JG000369, 2007.a

509 Frey, K. E., Siegel, D. I., and Smith, L. C.: Geochemistry of west Siberian streams and
510 their potential response to permafrost degradation, *Water Resour. Res.*, 43(3),
511 doi:10.1029/2006WR004902, 2007.b

512 Golovatskaya, E. A., and Lyapina, E. E.: Distribution of total mercury in peat soil profiles
513 in West Siberia, *Contemp. Probl. Ecol.*, 2(2), 156–161, doi:10.1134/S199542550902012X, 2009.

514 Hararuk, O., Obrist, D., and Luo, Y.: Modelling the sensitivity of soil mercury storage to
515 climate-induced changes in soil carbon pools, *Biogeosciences*, 10(4), 2393–2407, doi:10.5194/bg-
516 10-2393-2013, 2013.

517 Hugelius, G., Strauss, J., Zubrzycki, S., Harden, J. W., Schuur, E. A. G., Ping, C. L.,
518 Schirrmeister, L., Grosse, G., Michaelson, G. J., Koven, C. D., O'Donnell, J. A., Elberling, B.,
519 Mishra, U., Camill, P., Yu, Z., Palmtag, J., and Kuhry, P.: Estimated stocks of circumpolar
520 permafrost carbon with quantified uncertainty ranges and identified data gaps, *Biogeosciences*,
521 11(23), 6573–6593, doi:10.5194/bg-11-6573-2014, 2014.

522 Jensen, A., and Jensen, A.: Historical deposition rates of mercury in scandinavia estimated
523 by dating and measurement of mercury in cores of peat bogs, *Water, Air, Soil Pollut.*, 56(1), 769–
524 777, doi:10.1007/BF00342315, 1991.

525 Jiskra, M., Sonke, J. E., Agnan, Y., Helming, D., and Obrist, D.: Insights from mercury
526 stable isotopes on terrestrial–atmosphere exchange of Hg(0) in the Arctic tundra, *Biogeosciences*,
527 16(20), 4051–4064, doi:10.5194/bg-16-4051-2019, 2019.

528 Jiskra, M., Sonke, J. E., Obrist, D., Bieser, J., Ebinghaus, R., Myhre, C. L., Pfaffhuber, K.
529 A., Wängberg, I., Kyllonen, K., Worthy, D., Martin, L. G., Labuschagne, C., Mkololo, T.,
530 Ramonet, M., Magand, O., and Dommergue, A.: A vegetation control on seasonal variations in
531 global atmospheric mercury concentrations, *Nat. Geosci.*, 11(4), 244–250, doi:10.1038/s41561-
532 018-0078-8, 2018.

533 Kremenetski, K. V., Velichko, A. A., Borisova, O. K., MacDonald, G. M., Smith, L. C.,
534 Frey, K. E., and Orlova, L. A.: Peatlands of the Western Siberian lowlands: Current knowledge
535 on zonation, carbon content and Late Quaternary history, *Quat. Sci. Rev.*, 22(5–7), 703–723,
536 doi:10.1016/S0277-3791(02)00196-8, 2003.

537 Kurina, I.V., and Veretennikova, E.E.: Impact of climate change of the Holocene on the
538 development of the ridge-hollow swamp complex of Western Siberia, *Izvestiya Rossiiskoi
539 Akademii Nauk, Seriya Geograficheskaya*, 2, 74-87, <https://doi.org/10.15356/0373-2444-2015-2-74-87>, 2015. (In Russian).

541 Kurina, I.V., Veretennikova, E.E., Il'ina, A.A., Dyukarev, E.A., Golovatskaya, E.A., and
542 Smirnov, S.V.: Reconstruction of conditions of formation of the eutrophic peatland deposits in
543 south of the taiga zone of Western Siberia, *Izvestiya Rossiiskoi Akademii Nauk, Seriya
544 Geograficheskaya*, 4, 66-76, <https://doi.org/10.1134/S2587556618040106>, 2018.

545 Lim, A. G., Sonke, J. E., Krickov, I. V., Manasypov, R. M., Loiko, S. V., and Pokrovsky,
546 O. S.: Enhanced particulate Hg export at the permafrost boundary, western Siberia, *Environ.*
547 *Pollut.*, 254, doi:10.1016/j.envpol.2019.113083, 2019.

548 Loiko, S., Raudina, T., Lim, A., Kuzmina, D., Kulizhskiy, S., and Pokrovsky, O.:
549 Microtopography controls of carbon and related elements distribution in the West Siberian frozen
550 bogs, *Geosciences*, 9(7), 291, doi:10.3390/geosciences9070291, 2019.

551 Lyapina, E. E., Golovatskaya, E. A., and Ippolitov, I. I.: Mercury concentration in natural
552 objects of west Siberia, *Contemp. Probl. Ecol.*, 2(1), 1–5, doi:10.1134/S1995425509010019,
553 2009.

554 Melendez-Perez, J. J., Fostier, A. H., Carvalho, J. A., Windmöller, C. C., Santos, J. C., and
555 Carpi, A.: Soil and biomass mercury emissions during a prescribed fire in the Amazonian rain
556 forest, *Atmos. Environ.*, 96, 415–422, doi:10.1016/j.atmosenv.2014.06.032, 2014.

557 Morel, F. M. M., Kraepiel, A. M. L., and Amyot, M.: The chemical cycle and
558 bioaccumulation of mercury, *Annu. Rev. Ecol. Syst.*, 29, 543–566,
559 doi:10.1146/annurev.ecolsys.29.1.543, 1998.

560 Morgalev, Y. N., Lushchaeva, I. V., Morgaleva, T. G., Kolesnichenko, L. G., Loiko, S. V.,
561 Krickov, I. V., Lim, A., Raudina, T. V., Volkova, I. I., Shirokova, L. S., Morgalev, S. Y.,
562 Vorobyev, S. N., Kirpotin, S. N., and Pokrovsky, O. S.: Bacteria primarily metabolize at the active
563 layer/permafrost border in the peat core from a permafrost region in western Siberia, *Polar Biol.*,
564 40(8), 1645–1659, doi:10.1007/s00300-017-2088-1, 2017.

565 Nadyozhina, E.D., Shkolnik, I.M., Pavlova, T.V., Molkentin, E.K., and Semioshina, A.A.:
566 Permafrost response to the climate warming as simulated by the regional climate model of the
567 main geophysical observatory, *Earth's Cryosphere*, XII 3, 3–11, 2008. (In Russian).

568 Obrist, D., Agnan, Y., Jiskra, M., Olson, C. L., Colegrove, D. P., Hueber, J., Moore, C.
569 W., Sonke, J. E., and Helmig, D.: Tundra uptake of atmospheric elemental mercury drives Arctic
570 mercury pollution, *Nature*, 547(7662), 201–204, doi:10.1038/nature22997, 2017.

571 Olson, C., Jiskra, M., Biester, H., Chow, J., and Obrist, D.: Mercury in Active-Layer
572 Tundra Soils of Alaska: Concentrations, Pools, Origins, and Spatial Distribution, *Global*
573 *Biogeochem. Cycles*, 32(7), 1058–1073, doi:10.1029/2017GB005840, 2018.

574 Osterwalder, S., Bishop, K., Alewell, C., Fritsche, J., Laudon, H., Åkerblom, S., and
575 Nilsson, M. B.: Mercury evasion from a boreal peatland shortens the timeline for recovery from
576 legacy pollution, *Scientific Reports*, 7, 16022, 10.1038/s41598-017-16141-7, 2017.

577 Osterwalder, S., Sommar, J., Åkerblom, S., Jocher, G., Fritsche, J., Nilsson, M. B., Bishop,
578 K., and Alewell, C.: Comparative study of elemental mercury flux measurement techniques over
579 a Fennoscandian boreal peatland, *Atmos. Environ.*, 172, 16–25,
580 doi:10.1016/j.atmosenv.2017.10.025, 2018.

581 Outridge, P. M., Macdonald, E. R. W., Wang, G. F., Stern, G. A., and Dastoor, A. P.: A
582 mass balance inventory of mercury in the Arctic Ocean, *Environ. Chem.*, 5, 89–111,
583 doi:10.1071/EN08002, 2008.

584 Panova, N. K., Trofimova, S. S., Antipina, T. G., Zinoviev, E. V., Gilev, A. V., and
585 Erokhin, N. G.: Holocene dynamics of vegetation and ecological conditions in the southern Yamal
586 Peninsula according to the results of comprehensive analysis of a relict peat bog deposit, *Russ. J.*
587 *Ecol.*, 41(1), 20–27, doi:10.1134/S1067413610010042, 2010.

588 Pavlov, A.V., and Malkova, G.V.: Mapping of trends of the contemporary ground
589 temperature changes in the Russian north, *Earth's Cryosphere*, XIII 4, 32–39, 2009. (In Russian).

590 Pearson, C., Howard, D., Moore, C., and Obrist, D.: Mercury and trace metal wet
591 deposition across five stations in Alaska: controlling factors, spatial patterns, and source regions,
592 *Atmos. Chem. Phys.*, 19(10), 6913–6929, doi:10.5194/acp-19-6913-2019, 2019.

593 Peregon, A., Maksyutov, S., and Yamagata, Y.: An image-based inventory of the spatial
594 structure of West Siberian wetlands, *Environ. Res. Lett.*, 4(4), doi:10.1088/1748-
595 9326/4/4/045014, 2009.

596 Peregon, A., Maksyutov, S., Kosykh, N. P., and Mironycheva-Tokareva, N. P.: Map-based
597 inventory of wetland biomass and net primary production in western Siberia, *J. Geophys. Res.*
598 *Biogeosciences*, 113(1), doi:10.1029/2007JG000441, 2008.

599 Pokrovsky, O. S., Manasypov, R. M., Loiko, S. V., Krickov, I. A., Kopysov, S. G.,
600 Kolesnichenko, L. G., Vorobyev, S. N., and Kirpotin, S. N.: Trace element transport in western
601 Siberian rivers across a permafrost gradient, *Biogeosciences*, 13(6), 1877–1900, doi:10.5194/bg-
602 13-1877-2016, 2016.

603 Pokrovsky, O. S., Manasypov, R. M., Loiko, S., Shirokova, L. S., Krickov, I. A.,
604 Pokrovsky, B. G., Kolesnichenko, L. G., Kopysov, S. G., Zemtsov, V. A., Kulizhsky, S. P.,
605 Vorobyev, S. N., and Kirpotin, S. N.: Permafrost coverage, watershed area and season control of
606 dissolved carbon and major elements in western Siberian rivers, *Biogeosciences*, 12(21), 6301–
607 6320, doi:10.5194/bg-12-6301-2015, 2015.

608 Ponomareva, O.E., Gravis, A.G., and Berdnikov, N.M.: Contemporary dynamics of frost
609 mounds and flat peatlands in north taiga of West Siberia (on the example of Nadym site), *Earth's*
610 *Cryosphere*, 16, 21–30, 2012. (In Russian).

611 Preis, Y., and Karpenko, L.V.: Detailed reconstruction of bog functional state as a response
612 to continental climate changes in Holocene (the middle taiga of Western Siberia), *Bulletin of the*
613 *Tomsk Polytechnic University, Geo Assets Engineering*, 326 (2), 90-102, 2015. (In Russian).

614 Prietzel, J., Tyufekchieva, N., Eusterhues, K., Kögel-Knabner, I., Thieme, J., Paterson, D.,
615 McNulty, I., de Jonge, M., Eichert, D., and Salomé, M.: Anoxic versus oxic sample pretreatment:
616 Effects on the speciation of sulfur and iron in well-aerated and wetland soils as assessed by X-ray
617 absorption near-edge spectroscopy (XANES), *Geoderma*, 153(3–4), 318–330,
618 doi:10.1016/j.geoderma.2009.08.015, 2009.

619 Raudina, T. V., Loiko, S. V., Lim, A. G., Krickov, I. V., Shirokova, L. S., Istigechev, G.
620 I., Kuzmina, D. M., Kulizhsky, S. P., Vorobyev, S. N., and Pokrovsky, O. S.: Dissolved organic
621 carbon and major and trace elements in peat porewater of sporadic, discontinuous, and continuous
622 permafrost zones of western Siberia, *Biogeosciences*, 14(14), 3561–3584, doi:10.5194/bg-14-
623 3561-2017, 2017.

624 Romanovsky, V. E., Smith, S. L., and Christiansen, H. H.: Permafrost thermal state in the
625 polar Northern Hemisphere during the international polar year 2007–2009: a synthesis, *Permafrost*
626 *periglac*, 21(2), 106-116, <https://doi.org/10.1002/ppp.683>, 2010.

627 Romanovsky, V.E., Kholodov, A.L., Marchenko, S.S., Oberman, N.G., Drozdov, D.S.,
628 Malkova, G.V., Moskalenko, N.G., Vasiliev, A. A., Sergeev, D. O., and Zheleznyak, M. N.:
629 Thermal State and Fate of Permafrost in Russia: First Results of IPY, in: *Proceedings of the 9th*
630 *International Conference on Permafrost*, edited by: Kane, D.L., and Hinkel, K.M., University of
631 Alaska, Fairbanks, June 29 – July 3, 2008 , vol. 2, 1511–1518, 2008.

632 Roulet, M., Lucotte, M., Canuel, R., Farella, N., Courcelles, M., Guimaraes, J. R. D.,
633 Mergler, D., and Amorim, M.: Increase in mercury contamination recorded in lacustrine sediments
634 following deforestation in the central Amazon, *Chem. Geol.*, 165(3–4), 243–266,
635 doi:10.1016/S0009-2541(99)00172-2, 2000.

636 Roulet, M., Lucotte, M., Saint-Aubin, A., Tran, S., Rhéault, I., Farella, N., De Jesus Da
637 Silva, E., Dezencourt, J., Sousa Passos, C. J., Santos Soares, G., Guimaraes, J. R. D., Mergler, D.,
638 and Amorim, M.: The geochemistry of mercury in central Amazonian soils developed on the
639 Alter-do-Chao formation of the lower Tapajos River Valley, Para state, Brazil, *Sci. Total Environ.*,
640 223(1), 1–24, doi:10.1016/S0048-9697(98)00265-4, 1998.

641 Rudmin, M., Ruban, A., Savichev, O., Mazurov, A., Dauletova, A., and Savinova, O.:
642 Authigenic and detrital minerals in peat environment of Vasyugan swamp, western Siberia,
643 Minerals, 8(11), doi:10.3390/min8110500, 2018.

644 Rydberg, J., Klaminder, J., Rosén, P., and Bindler, R.: Climate driven release of carbon
645 and mercury from permafrost mires increases mercury loading to sub-arctic lakes, Sci. Total
646 Environ., 408(20), 4778–4783, doi:10.1016/j.scitotenv.2010.06.056, 2010.

647 Schuster, P. F., Schaefer, K. M., Aiken, G. R., Antweiler, R. C., Dewild, J. F., Gryziec, J.
648 D., Gusmeroli, A., Hugelius, G., Jafarov, E., Krabbenhoft, D. P., Liu, L., Herman-Mercer, N., Mu,
649 C., Roth, D. A., Schaefer, T., Striegl, R. G., Wickland, K. P., and Zhang, T.: Permafrost stores a
650 globally significant amount of mercury, Geophys. Res. Lett., 45(3), 1463–1471,
651 doi:10.1002/2017GL075571, 2018.

652 Selin, N. E., Jacob, D. J., Yantosca, R. M., Strode, S., Jaeglé, L., and Sunderland, E. M.:
653 Global 3-D land-ocean-atmosphere model for mercury: Present-day versus preindustrial cycles
654 and anthropogenic enrichment factors for deposition, Global Biogeochem. Cycles, 22(2),
655 doi:10.1029/2007GB003040, 2008.

656 Sheng, Y., Smith, L. C., MacDonald, G. M., Kremenetski, K. V., Frey, K. E., Velichko,
657 A. A., Lee, M., Beilman, D. W., and Dubinin, P.: A high-resolution GIS-based inventory of the
658 west Siberian peat carbon pool, Global Biogeochem. Cycles, 18(3), doi:10.1029/2003GB002190,
659 2004.

660 Shevchenko, V. P., Pokrovsky, O. S., Vorobyev, S. N., Krickov, I. V., Manasypov, R. M.,
661 Politova, N. V., Kopysov, S. G., Dara, O. M., Auda, Y., Shirokova, L. S., Kolesnichenko, L. G.,
662 Zemtsov, V. A., and Kirpotin, S. N.: Impact of snow deposition on major and trace element
663 concentrations and elementary fluxes in surface waters of the Western Siberian Lowland across a
664 1700'km latitudinal gradient, Hydrol. Earth Syst. Sci., 21(11), 5725–5746, doi:10.5194/hess-21-
665 5725-2017, 2017.

666 Skyllberg, U., Qian, J., Frech, W., Xia, K., and Bleam, W. F.: Distribution of mercury,
667 methyl mercury and organic sulphur species in soil, soil solution and stream of a boreal forest
668 catchment, Biogeochemistry, 64(1), 53–76, doi:10.1023/A:1024904502633, 2003.

669 Smieja-Król, B., Fiałkiewicz-Kozięł, B., Sikorski, J., and Palowski, B.: Heavy metal
670 behaviour in peat - A mineralogical perspective, Sci. Total Environ., 408(23), 5924–5931,
671 doi:10.1016/j.scitotenv.2010.08.032, 2010.

672 Smith-Downey, N. V., Sunderland, E. M., and Jacob, D. J.: Anthropogenic impacts on
673 global storage and emissions of mercury from terrestrial soils: Insights from a new global model,
674 J. Geophys. Res., 115(G3), G03008, doi:10.1029/2009JG001124, 2010.

675 Soerensen, A. L., Jacob, D. J., Schartup, A. T., Fisher, J. A., Lehnher, I., St Louis, V. L.,
676 Heimbürger, L. E., Sonke, J. E., Krabbenhoft, D. P., and Sunderland, E. M.: A mass budget for
677 mercury and methylmercury in the Arctic Ocean, Global Biogeochem. Cycles, 30(4), 560–575,
678 doi:10.1002/2015GB005280, 2016.

679 Sonke, J. E., Teisserenc, R., Heimbürger-Boavida, L. E., Petrova, M. V., Maruszak, N.,
680 Le Dantec, T., Chupakov, A. V., Li, C., Thackray, C. P., Sunderland, E. M., Tananaev, N., and
681 Pokrovsky, O. S.: Eurasian river spring flood observations support net Arctic Ocean mercury
682 export to the atmosphere and Atlantic Ocean, Proc. Natl. Acad. Sci. U. S. A., 115(50), E11586–
683 E11594, doi:10.1073/pnas.1811957115, 2018.

684 St. Pierre, K. A., St. Louis, V. L., Lehnher, I., Gardner, A. S., Serbu, J. A., Mortimer, C.
685 A., Muir, D. C. G., Wiklund, J. A., Lemire, D., Szostek, L., and Talbot, C.: Drivers of mercury
686 cycling in the rapidly changing glacierized watershed of the High Arctic's largest lake by volume
687 (Lake Hazen, Nunavut, Canada), Environ. Sci. Technol., 53(3), 1175–1185,
688 doi:10.1021/acs.est.8b05926, 2019.

689 Steffen, A., Douglas, T., Amyot, M., Ariya, P., Aspmo, K., Berg, T., Bottenheim, J.,
690 Brooks, S., Cobbett, F., Dastoor, A., Dommergue, A., Ebinghaus, R., Ferrari, C., Gardfeldt, K.,

691 Goodsite, M. E., Lean, D., Poulain, A. J., Scherz, C., Skov, H., Sommar, J., and Temme, C.: A
692 synthesis of atmospheric mercury depletion event chemistry in the atmosphere and snow, *Atmos.*
693 *Chem. Phys.*, 8(6), 1445–1482, doi:10.5194/acp-8-1445-2008, 2008.

694 Steinmann, P., and Shotyk, W.: Chemical composition, pH, and redox state of sulfur and
695 iron in complete vertical porewater profiles from two Sphagnum peat bogs, Jura Mountains,
696 Switzerland, *Geochim. Cosmochim. Acta*, 61(6), 1143–1163, doi:10.1016/S0016-
697 7037(96)00401-2, 1997.

698 Stepanova, V. A., Pokrovsky, O. S., Viers, J., Mironycheva-Tokareva, N. P., Kosykh, N.
699 P., and Vishnyakova, E. K.: Elemental composition of peat profiles in western Siberia: Effect of
700 the micro-landscape, latitude position and permafrost coverage, *Appl. Geochemistry*, 53, 53–70,
701 doi:10.1016/j.apgeochem.2014.12.004, 2015.

702 Stern, G. A., Macdonald, R. W., Outridge, P. M., Wilson, S., Chételat, J., Cole, A.,
703 Hintelmann, H., Loseto, L. L., Steffen, A., Wang, F., and Zdanowicz, C.: How does climate
704 change influence arctic mercury?, *Sci. Total Environ.*, 414, 22–42,
705 doi:10.1016/j.scitotenv.2011.10.039, 2012.

706 Talbot, J., Moore, T. R., Wang, M., Ouellet Dallaire, C., and Riley, J. L.: Distribution of
707 lead and mercury in Ontario peatlands, *Environ. Pollut.*, 231, 890–898,
708 doi:10.1016/j.envpol.2017.08.095, 2017.

709 Tamocai, C., Canadell, J. G., Schuur, E. A. G., Kuhry, P., Mazhitova, G., and Zimov, S.:
710 Soil organic carbon pools in the northern circumpolar permafrost region, *Global Biogeochem.*
711 *Cycles*, 23(2), 1–11, doi:10.1029/2008GB003327, 2009.

712 Trofimova, I. E., and Balybina, A. S.: Classification of climates and climatic
713 regionalization of the West-Siberian plain, *Geogr. Nat. Resour.*, 35(2), 114–122,
714 doi:10.1134/S1875372814020024, 2014.

715 Vasilevich, R. S.: Major and Trace Element Compositions of Hummocky Frozen Peatlands
716 in the Forest–Tundra of Northeastern European Russia, *Geochemistry International*, 56, 1276–
717 1288, doi:10.1134/S0016702918100129, 2018.

718 Velichko, A. A., Timireva, S. N., Kremenetski, K. V., MacDonald, G. M., and Smith, L.
719 C.: West Siberian Plain as a late glacial desert, *Quat. Int.*, 237(1–2), 45–53,
720 doi:10.1016/j.quaint.2011.01.013, 2011.

721 Vishnyakova, E.K., and Mironycheva-Tokareva, N.P.: Moss decomposition in Western
722 Siberian mires, in: *Mosses: Ecology, Life Cycle and Significance*, edited by: Pokrovsky, O.,
723 Volkova, I., Kosykh, N., and Shevchenko, V., 4th ed. Nova Science Publishers Inc. New York,
724 pp. 217–241, 2018.

725 Vorobyev, S. N., Pokrovsky, O. S., Serikova, S., Manasypov, R. M., Krickov, I. V.,
726 Shirokova, L. S., Lim, A., Kolesnichenko, L. G., Kirpotin, S. N., and Karlsson, J.: Permafrost
727 boundary shift in Western Siberia may not modify dissolved nutrient concentrations in rivers,
728 *Water* (Switzerland), 9(12), doi:10.3390/w9120985, 2017.

729 Wang, X., Yuan, W., Lin, C.-J., Zhang, L., Zhang, H., and Feng, X.: Climate and
730 vegetation as primary drivers for global mercury storage in surface soil, *Environ. Sci. Technol.*,
731 53(18), 10665–10675, doi:10.1021/acs.est.9b02386, 2019.

732 Wilhelm, R. C., Niederberger, T. D., Greer, C., and Whyte, L. G.: Microbial diversity of
733 active layer and permafrost in an acidic wetland from the Canadian high arctic, *Can. J. Microbiol.*,
734 57(4), 303–315, doi:10.1139/w11-004, 2011.

735 Zhang, Y., Jacob, D. J., Dutkiewicz, S., Amos, H. M., Long, M. S., and Sunderland, E. M.:
736 Biogeochemical drivers of the fate of riverine mercury discharged to the global and Arctic oceans,
737 *Global Biogeochem. Cycles*, 29(6), 854–864, doi:10.1002/2015GB005124, 2015.

738 Zolkos, S., Krabbenhoft, D. P., Suslova, A., Tank, S. E., McClelland, J. W., Spencer, R.
739 G. M., Shiklomanov, A., Zhulidov, A. V., Gurtovaya, T., Zimov, N., Zimov, S., Mutter, E. A.,

740 Kutny, L., Amos, E. and Holmes, R. M.: Mercury export from Arctic great rivers, Environ. Sci.
741 Technol., doi:10.1021/acs.est.9b07145, 2020.
742

743 **Table 1.** Mean (\pm SD) concentrations and stocks of C and Hg in 6 studied sites of Western
 744 Siberia Lowlands (WSL) peatbogs.

745

Horizons	C, %	Hg, ng g ⁻¹	kg C m ⁻²	mg Hg m ⁻²	R _{HgC} (Gg Pg ⁻¹)
Plotnikovo (Pl), Southern taiga, 56.9°N*					
ALT (0-140 cm)	45±2	36±12	24	2.8	0.08±0.03
Mineral (140-150 cm)	13	53	23	9.0	0.40
Total (150 cm)	43±8	37±12	47	11.8	0.10±0.09
0-30 cm	44±2	44±5	3	0.3	0.10±0.01
0-100 cm	45±2	36±10	9	0.8	0.08±0.02
Mukhrino (Mh), Middle taiga, 60.9°N*					
ALT (0-360 cm)	53±7	26±13	67	4.3	0.05±0.03
Mineral (360-380 cm)	15±19	24±19	51	8.3	0.46±0.46
Total (380 cm)	51±10	26±19	118	12.6	0.07±0.12
0-30 cm	50±0.4	29±7	4	0.3	0.06±0.02
0-100 cm	52±5	32±17	18	1.3	0.06±0.04
Kogalym (Kg), Northern taiga, 62.3°N*					
ALT (0-175 cm)	48±4	48±30	93	8.7	0.10±0.06
Mineral (175-190 cm)	10±13	12±10	17	2.3	0.34±0.36
Total (190 cm)	45±12	45±30	110	11	0.12±0.12
0-30 cm	45±1	65±19	3	0.5	0.14±0.04
0-100 cm	47±2	49±34	38	3	0.11±0.07
Khanymey (Kh), Northern taiga, 63.8°N					
ALT (0-34 cm)	44±2	64±43	17	2.1	0.15±0.10
PF1 (34-100 cm)	50±2	47±13	78	7.6	0.09±0.02
PF2 (34-138 cm)	48±6	47±11	119	11.8	0.10±0.02
Mineral (138-147 cm)	1±1	4±1	2	0.5	0.31±0.13
Total (147 cm)	42±16	47±28	138	14.4	0.13±0.09
0-30 cm	43±1	71±46	13	1.8	0.17±0.11
0-100 cm	47±4	54±29	95	9.6	0.12±0.07
Pangody (Pg), Forest tundra, 65.9°N					
ALT (0-40 cm)	50±4	78±25	38	5.3	0.16±0.07
PF1 (40-100 cm)	53±4	61 ±25	54	6.6	0.11±0.04
PF2 (40-155 cm)	48±10	67±23	78	11.0	0.15±0.07
Mineral (155-185 cm)	3±1	24±11	15	12.5	0.88±0.28
Total (185 cm)	41±19	62±28	130	28.8	0.27±0.30
0-30 cm	50±5	83±26	26	4.0	0.17±0.07
0-100 cm	52±4	68±25	92	11.9	0.13±0.06
Tazovsky (Tz), Southern tundra, 67.4°N					
ALT (0-40 cm)	49±3	186±110	22	7.4	0.38±0.20
PF1 (40-100 cm)	46±3	109±28	27	6.3	0.23±0.06
PF2 (40-380 cm)	47±4	104±39	156	35.0	0.22±0.08
Mineral (380-405 cm)	14±5	152±65	60	64.7	1.24±0.66
Total (405 cm)	45±9	115±57	238	107.0	0.30±0.31
0-30 cm	49±4	209±120	16	6.0	0.42±0.21
0-100 cm	47±3	140±80	48	13.7	0.29±0.15

746

747 **Footnote:** ALT is Active Layer Thickness; PF1 is frozen peat, (ALT-100 cm); PF2 is frozen peat
 748 (ALT to mineral layer); 'Mineral' is mineral layer; 'Total' is total Hg content averaged over full
 749 sampled depth. *In permafrost-free zone, the ALT extends from the surface to the mineral layer.

750

751

752

753 **Table 2.** Estimated pan-Arctic permafrost soil Hg inventory (Gg) for different depth ranges
 754 down to 300 cm. Hg pool uncertainties are reported as the interquartile range (IQR), i.e. the 25th
 755 to 75th percentiles of the Hg pool distribution estimates by a Monte Carlo method. Soil organic
 756 carbon (SOC) pools are from Hugelius et al. (2014).

depth range	soils	SOC	Hg Pool	IQR		% of total
		Pg	Pg	Pg	Pg	
0-30 cm	organic (>20% SOC)	172	35	13	45	48
	mineral (<20% SOC)	45	37	15	47	52
	total	217	72	39	91	
0-100 cm	organic (>20% SOC)	253	50	26	65	21
	mineral (<20% SOC)	219	191	59	287	79
	total	472	240	110	336	
0-200 cm	organic (>20% SOC)	366	72	44	92	16
	mineral (<20% SOC)	461	392	196	529	84
	total	827	464	269	601	
0-300 cm	organic (>20% SOC)	427	85	55	106	14
	mineral (<20% SOC)	607	512	300	666	86
	total	1034	597	384	750	

757
 758
 759
 760

Table 3. Comparison of estimated pan-Arctic permafrost soil Hg pools by different studies.

depth range	Hugelius et al. 2014		Schuster et al. 2018		Olson et al. 2018		this study		
	SOC	95% CI	Hg Pool	95% CI	Hg Pool	25% CI	Hg Pool	IQR	
		Pg		Pg		Gg		Gg	Gg
0-30 cm	217	12	347	±196	26	21 - 42	72	39	- 91
0-100 cm	472	27	755	±301	184	136 - 274	240	110	- 336
0-200 cm	827	108	1323	±764			464	269	- 601
0-300 cm	1034	150	1656	±962			597	384	- 750

761

¹ Confidence interval (CI) corresponding to the 37.5th to 62.5th percentile

² interquartile range (IQR), i.e. the 25th to 75th percentiles

762
 763
 764
 765
 766
 767
 768
 769
 770
 771
 772
 773

774 **Table 4.** Estimated soil Hg pool (0 to 30 cm interval) for different climate zones based on
 775 reported R_{HgC} and carbon pools. Hg pool uncertainties are reported as the interquartile range
 776 (IQR), i.e. the 25th to 75th percentiles of the Hg pool distribution estimates by a Monte Carlo
 777 method.
 778

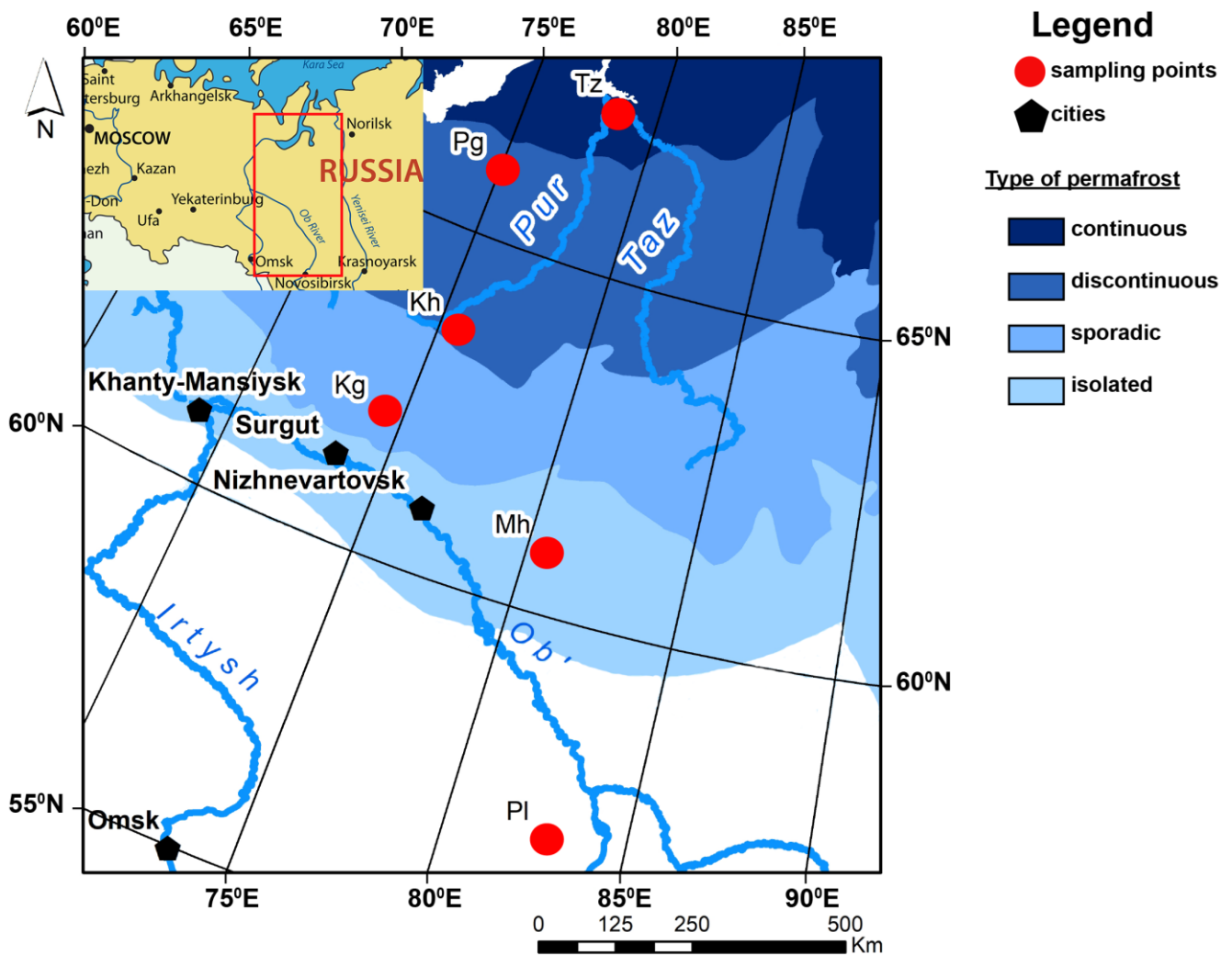
Climate zone	C pool Pg	median R_{HgC}	mean R_{HgC}	Hg pool Gg	IQR	
		(Gg/Pg)	(Gg/Pg)		Gg	
tropics	208	1.85	2.14	446	268	- 556
subtropics	102	1.83	2.13	217	128	- 271
temperate	191	1.37	1.55	296	183	- 366
boreal	140	0.35	0.41	55	35	- 67
arctic	217	(0.15, 0.64)	(0.19, 0.67)	72	39	- 91
total	858			1086	852	1265

779
 780 ¹ Carbon pools are from FAO and ITPS (2018).

781 ² The arctic R_{HgC} and Hg pool are from Table 2.

782 ³ The arctic carbon pool is from Hugelius et al. (2014)

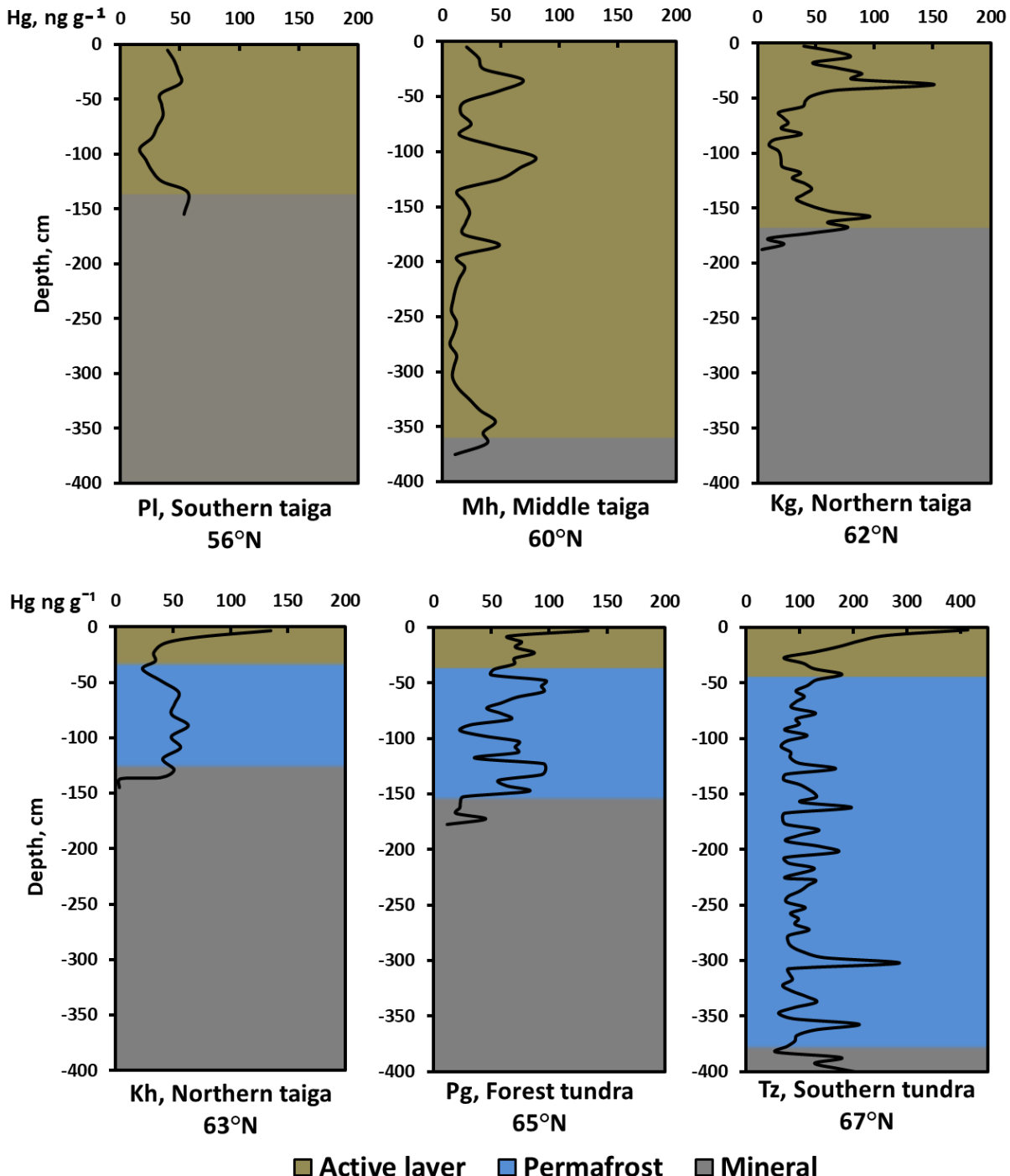
783
 784
 785
 786
 787
 788



789
790

791 **Fig. 1.** Sampling sites and permafrost boundaries (modified after Brown et al., 2001) of WSL
 792 territory investigated in this work. The climate and soil parameters of 6 sampling sites
 793 (Tazovsky Tz, Pangody Pg, Khanymey Kh, Kogalym Kg, Mukhrino Mh, and Plotnikovo Pl) are
 794 listed in Supplementary Table S1.

795
796



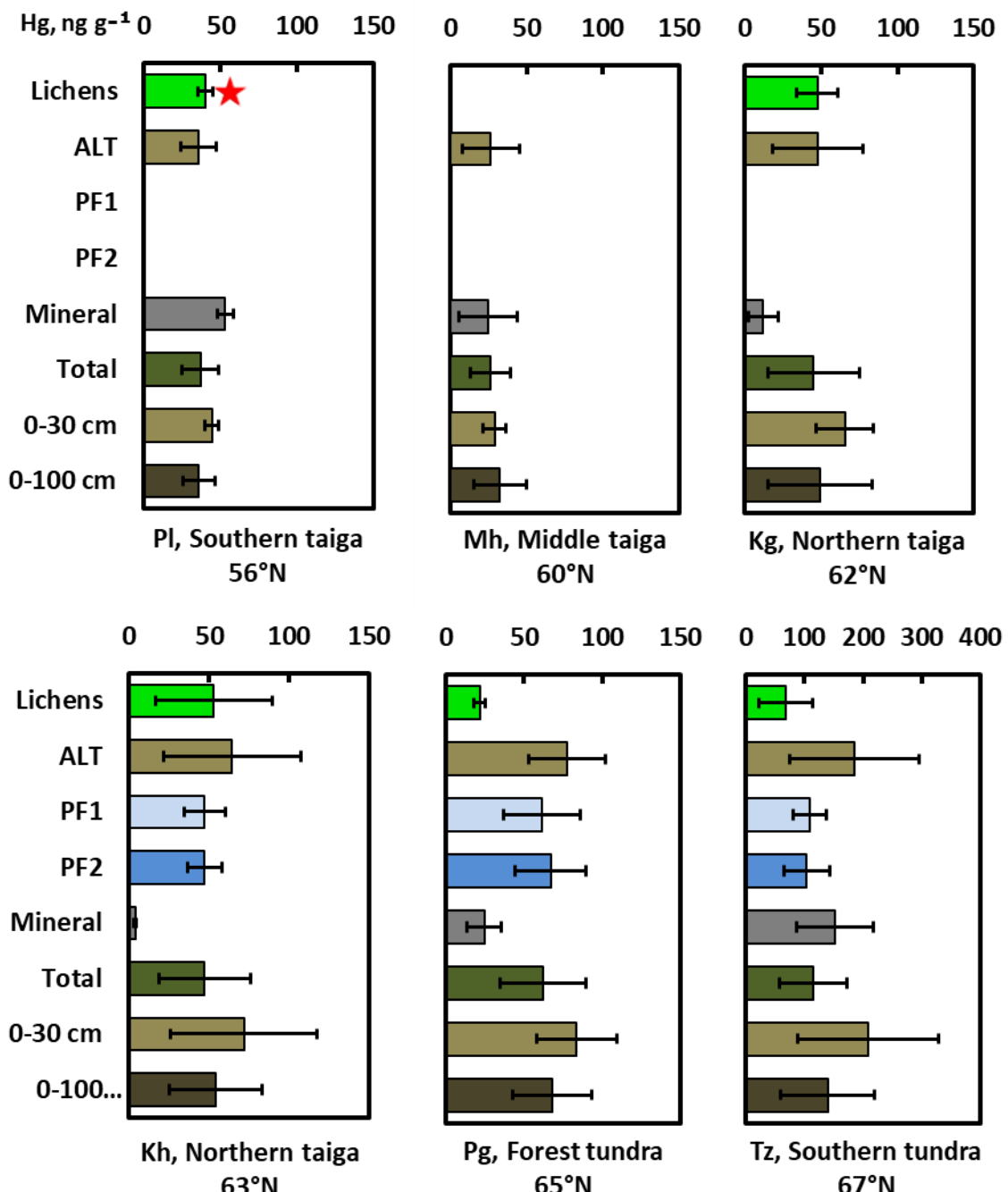
797
798

799

800 **Fig. 2.** Vertical depth profile distribution of total Hg (THg) in 6 peat cores across a 1700 km
801 latitudinal transect of the WSL. Site location and physio-geographical parameters are shown in
802 Fig. 1 and Table S1.

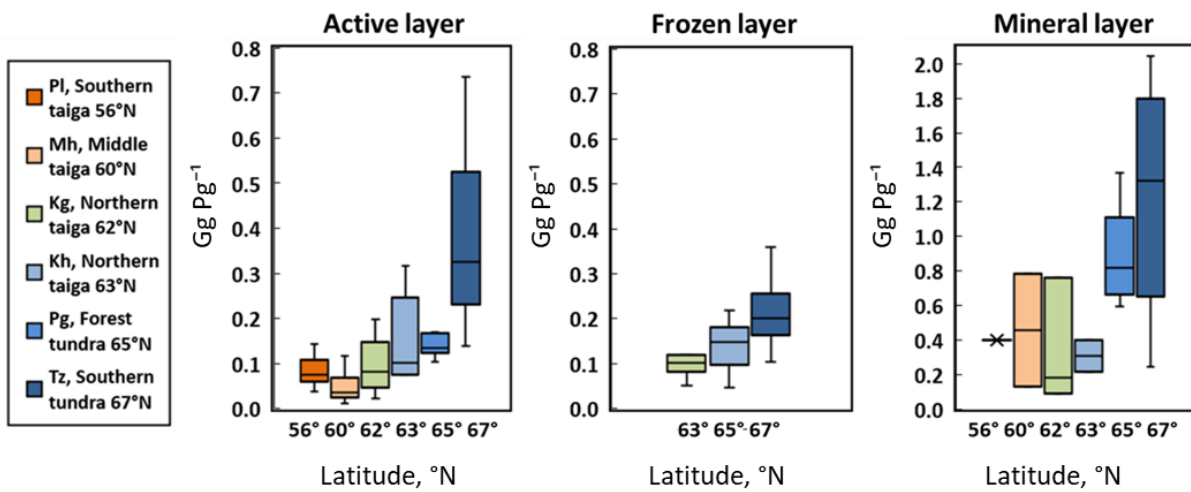
803

804

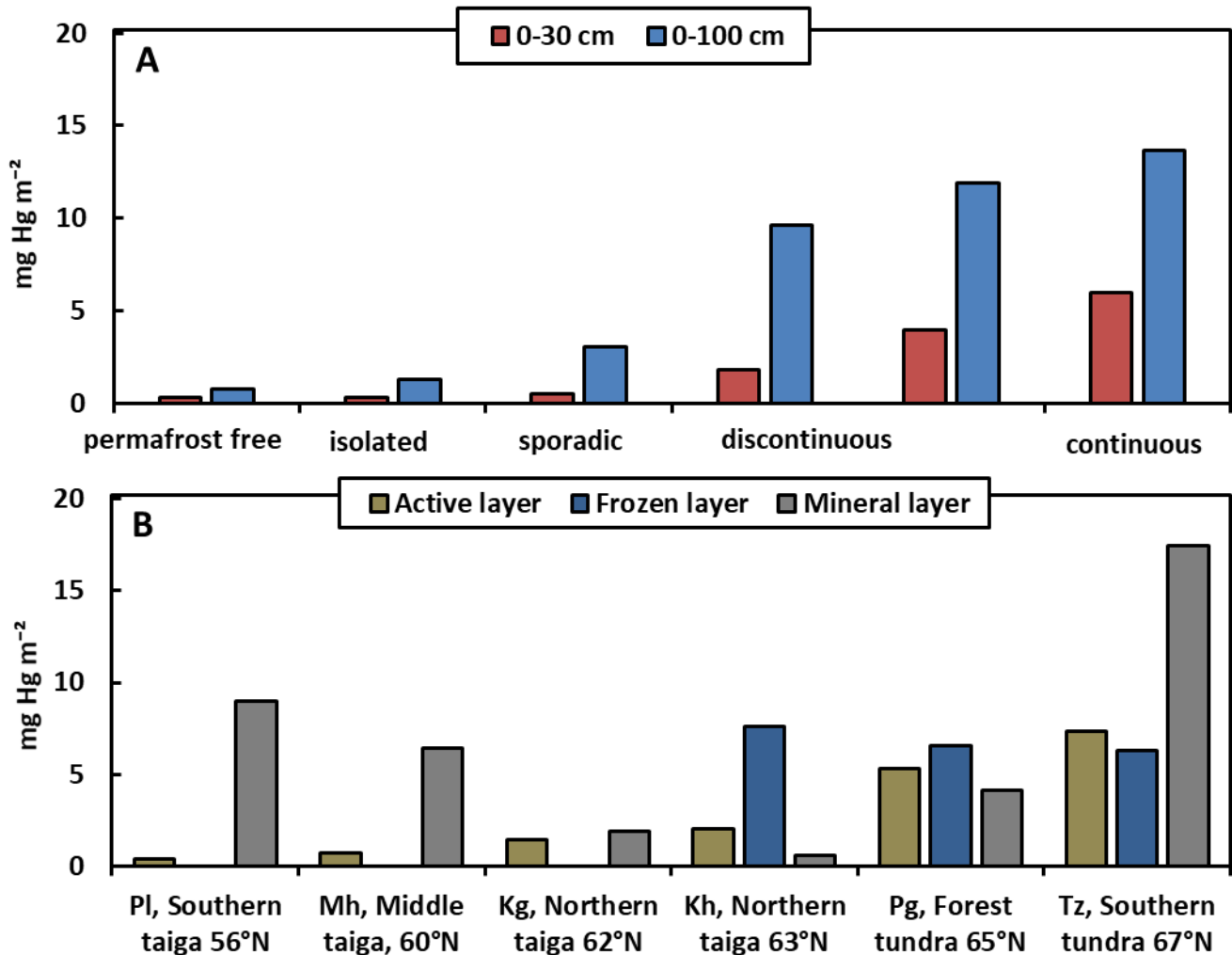


808 **Fig. 3.** Mean (\pm SD), depth-integrated Hg concentrations in peat columns and mineral layers of 6
809 studied sites. Red asterisk represents the data from Lyapina et al. (2009).

810 **Footnote:** ALT is Active Layer Thickness; PF1 is frozen peat, (ALT-100 cm); PF2 is frozen peat
811 (ALT to mineral layer); 'Mineral' is mineral layer; 'Total' is total Hg content averaged over full
812 sampled depth. *In permafrost-free zone, the ALT extends from the surface to the mineral layer.
813



819 **Fig. 4.** The ratio Hg:C (Gg Pg⁻¹), median±IQR, in the active layer, frozen peat and mineral
 820 horizons across the WSL latitudinal transect.



835

836

837

838

839 **Fig. 5.** Latitudinal variation in WSL soil Hg storage (mg Hg m^{-2}) in the 0-30 and 0-100 cm peat
 840 layer (**A**) and in the active, frozen and mineral layers (**B**). In the permafrost-free zone, the first 40
 841 cm were used to calculate Hg storage in the active layer. The permafrost peat layer is fixed from
 842 the lower boundary of the active (unfrozen) layer down to 100 cm. Finally, for the mineral layer
 843 we considered only the first 10 cm below peat deposits across the full latitudinal gradient of the
 844 WSL peatland.

845

846

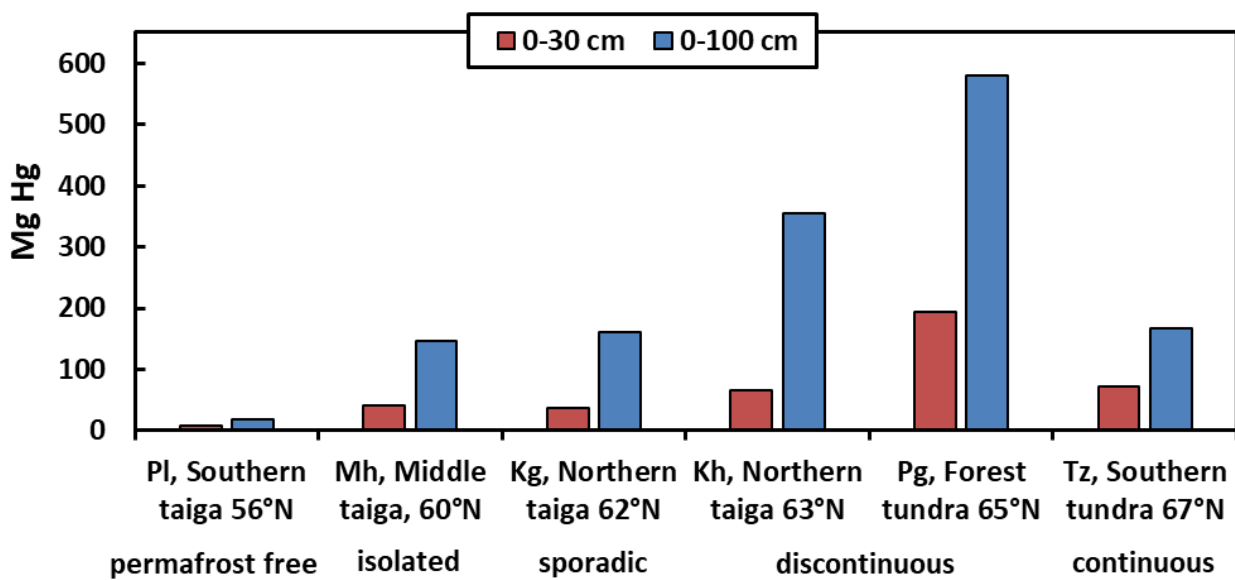
847

848

849

850

851
852
853



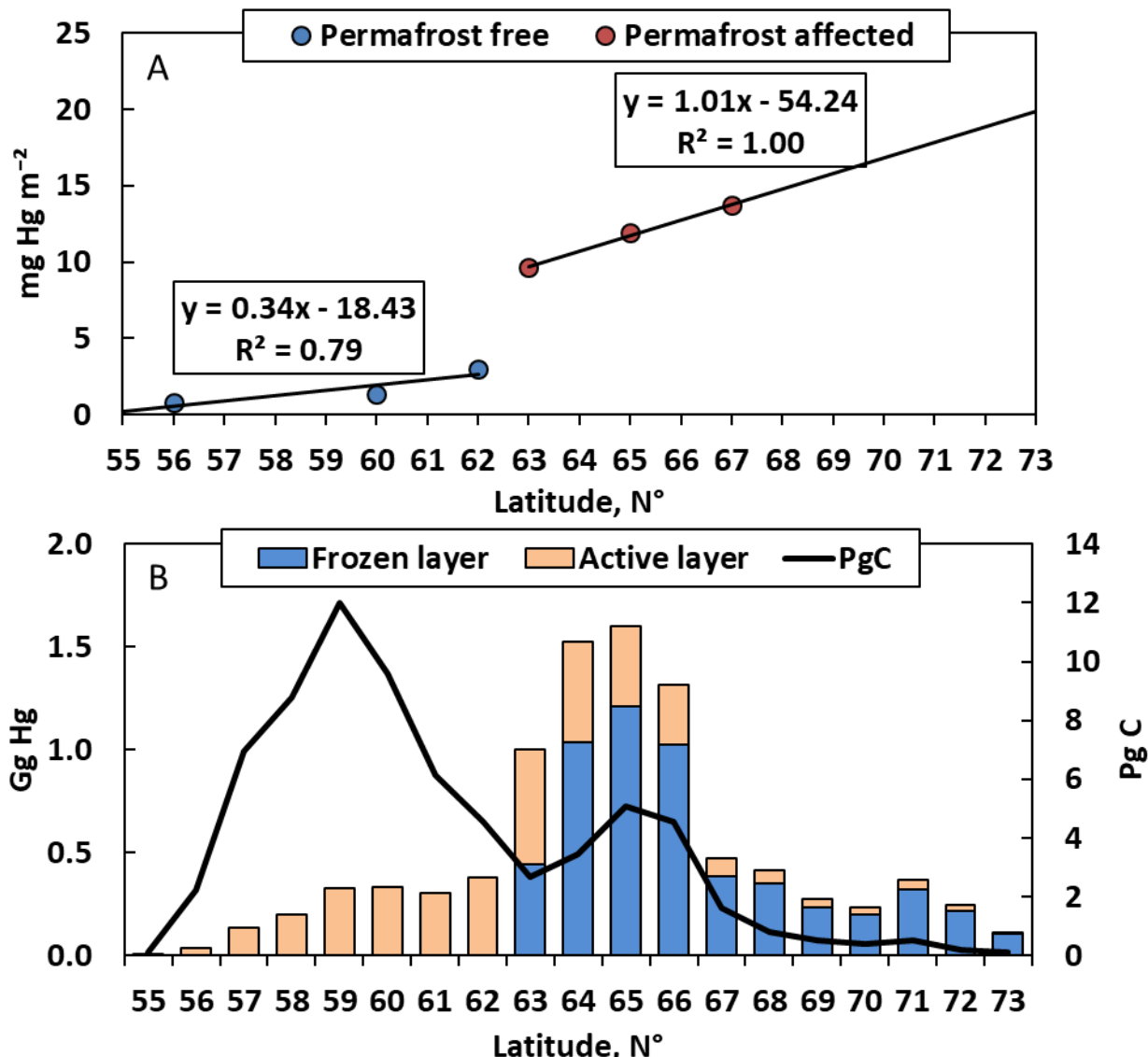
854

855

856

857 **Fig. 6.** Total, depth-integrated pools of Hg mass (Mg) in the upper 0-30 and 0-100 cm (red and
858 blue columns, respectively) of WSL frozen peatlands in each permafrost zone. The stocks are
859 calculated assuming the areal proportion of bogs from the landscape inventory across the WSL
860 (Sheng et al., 2004).

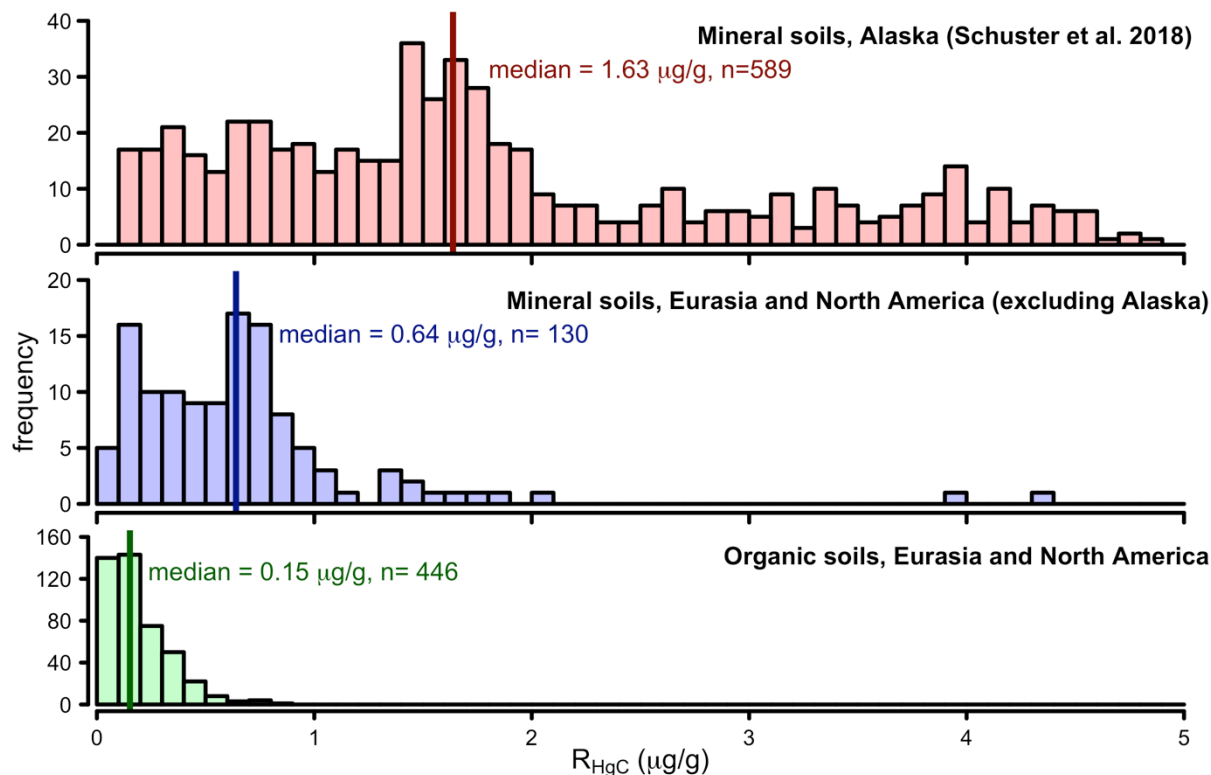
861



862
863
864
865
866
867
868
869
870
871
872
873
874

Fig. 7. Estimated Hg storage (mg Hg m^{-2}) in the 0-100 cm soil layer of the WSL (A) and latitudinal distribution of the Hg pool (Gg) in active and frozen peat layers of the WSL (B). Solid black line represents the WSL C pool (Pg) from Sheng et al. (2004).

875
876
877
878
879
880
881



882

883

884 **Fig. 8.** Histograms of published (Table S4) and WSL (this study) R_{HgC} data used for estimating
885 the northern circumpolar permafrost region soil Hg pool: top: Alaskan mineral soils (Schuster et
886 al., 2018), middle: mineral soils from Eurasia and North America (excluding Alaska), and
887 bottom: organic soils from Eurasia and North America (including Alaska).

888

889

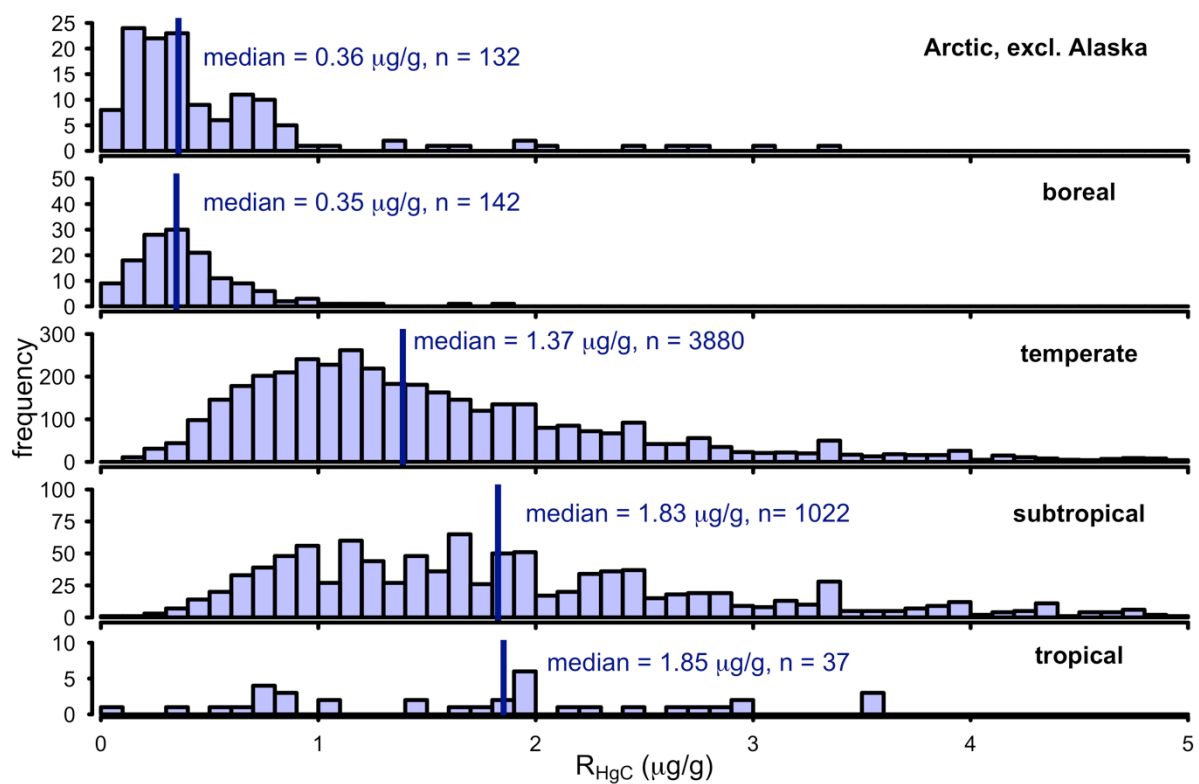
890

891

892

893

894



895

896

897

898 **Fig. 9.** Histograms and median R_{HgC} for the 0 - 30 cm soil interval for different global climate
 899 zones.
 900